



Article

Improved Thermophysical Properties and Energy Efficiency of Aqueous Ionic Liquid/MXene Nanofluid in a Hybrid PV/T Solar System

Likhan Das ¹, Khairul Habib ^{1,*}, R. Saidur ^{2,3}, Navid Aslfattahi ⁴ , Syed Mohd Yahya ⁵ and Fazlay Rubbi ¹

¹ Department of Mechanical Engineering, Universiti Teknologi PETRONAS, Bandar Seri Iskandar, Perak Darul Ridzuan 32610, Malaysia; likhan.das11@gmail.com (L.D.); mdfrs22@gmail.com (F.R.)

² Research Centre for Nanomaterials and Energy Technology (RCNMET), School of Science and Technology, Sunway University, Petaling Jaya 47500, Malaysia; saidur@sunway.edu.my

³ Department of Engineering, Lancaster University, Lancaster LA1 4YW, UK

⁴ Department of Mechanical Engineering, Faculty of Engineering, University of Malaya, Kuala Lumpur 50603, Malaysia; navid.fth87@yahoo.com

⁵ Sustainable Energy and Acoustics Research Lab, Mechanical Engineering Department, Aligarh Muslim University, Aligarh 202002, India; smyahya@zhcet.ac.in

* Correspondence: khairul.habib@utp.edu.my; Tel.: +60-102-442-375

Received: 21 May 2020; Accepted: 17 June 2020; Published: 14 July 2020



Abstract: In recent years, solar energy technologies have developed an emerging edge. The incessant research to develop a power source alternative to fossil fuel because of its scarcity and detrimental effects on the environment is the main driving force. In addition, nanofluids have gained immense interest as superior heat transfer fluid in solar technologies for the last decades. In this research, a binary solution of ionic liquid (IL) + water based ionanofluids is formulated successfully with two dimensional MXene (Ti_3C_2) nano additives at three distinct concentrations of 0.05, 0.10, and 0.20 wt % and the optimum concentration is used to check the performance of a hybrid solar PV/T system. The layered structure of MXene and high absorbance of prepared nanofluids have been perceived by SEM and UV-vis respectively. Rheometer and DSC are used to assess the viscosity and heat capacity respectively while transient hot wire technique is engaged for thermal conductivity measurement. A maximum improvement of 47% in thermal conductivity is observed for 0.20 wt % loading of MXene. Furthermore, the viscosity is found to rise insignificantly with addition of Ti_3C_2 by different concentrations. Conversely, viscosity decreases substantially as the temperature increases from 20 °C to 60 °C. However, based on their thermophysical properties, 0.20 wt % is found to be the optimum concentration. A comparative analysis in terms of heat transfer performance with three different nanofluids in PV/T system shows that, IL+ water/MXene ionanofluid exhibits highest thermal, electrical, and overall heat transfer efficiency compared to water/alumina, palm oil/MXene, and water alone. Maximum electrical efficiency and thermal efficiency are recorded as 13.95% and 81.15% respectively using IL + water/MXene, besides that, heat transfer coefficients are also noticed to increase by 12.6% and 2% when compared to water/alumina and palm oil/MXene respectively. In conclusion, it can be demonstrated that MXene dispersed ionanofluid might be great a prospect in the field of heat transfer applications since they can augment the heat transfer rate considerably which improves system efficiency.

Keywords: MXene; ionic liquid; nanofluids; thermophysical properties; PV/T system

1. Introduction

Since the industrial revolution, the demand for energy has been increasing day by day, thus it is anticipated that global energy demand will grow up to 30% by the year 2040 as stated in the *World Energy Report, 2019* by the International Energy Agency, (IEA) [1,2]. To meet this growing energy demand, fossil fuels are being burnt to a large extent, accounting for 87% of total energy supply. On this basis, the need for renewable energy resources is sought after due to the massive consumption of fossil fuels. Moreover, burning of these hydrocarbon deposits has a detrimental effect on the environment and global climate. Therefore, scientists are enforcing their efforts on proper utilization of green and renewable sources of energy mostly on solar, wind, tides, and geothermal energy [3]. Solar energy is considered the best alternative to supplement the consumption of fossil fuels in fulfilling energy demand. Furthermore, it is the most compelling source of renewable energy which can be utilized through numerous and ever-growing solar energy technologies—including solar thermal collectors, artificial photosynthesis, photovoltaics, solar ponds, and concentrating solar power plants [4–6]. Hybrid PV/T is a solar cogeneration approach that utilizes solar radiation and heat, producing both electrical and thermal energy. PV/T systems have gained immense popularity for residential and commercial applications because of their greenness and eco-friendly operation. The effectiveness of PV/T systems varies with several considerations such as incident angle of solar light, material, design, and working fluids [7,8]. Improving the thermal and optical properties of heat transfer fluid (HTF) is considered as the most convenient ways that augments the overall effectiveness of PV/T system. Water, thermal oil, ethylene glycol (EG), and ionic liquid are being employed as conventional working fluids in a hybrid solar PV/T system. Inclusion of solid nanoparticles into the heat transfer fluids can substantially improve optical and thermophysical properties [9–11]. The inclusion of nano-sized solid particles into base fluids, referred to as ‘nanofluids’, significantly alters thermophysical properties of the base liquids especially thermal conductivity [12–16]. Choi and Eastman [17] were the pioneers who coined the term “nanofluid”. Nanofluids have gained plenty of interest in recent decades as they have superior heat transport properties and also hold astounding possibilities in many clean engineering applications [18–20]; therefore, it is deemed to be the HTF for the next generation [21]. To date, researchers have conducted numerous investigations to improve the thermophysical properties of conventional HTFs by dispersing distinct nano additives such as metals, their carbides, oxides, or carbon nanotubes (CNTs) [22–24]. Recently, carbon-based nanoparticles and two-dimensional nanostructures have captivated ample attention due to their comparatively higher thermal conductivity, greater specific surface area, better compatibility with base fluid, better lubricating property, and ample availability when compared with other nanoparticles [25,26]. A broad number of studies were performed with graphite [27], carbon nanotubes (CNTs) [28,29], graphene [30], graphene oxide (GO) [31], nano diamond [32], and graphite flake [33] nanoparticles so far. Yu et al. [34] experimentally measured the thermal conductivity of EG based nanofluid with GO nanosheets where thermal conductivity was noticeably higher by 61% compared to pure EG, while the nanosheet concentration was 5 vol %. In another experimental work by Baby and Ramaprabhu [35], thermal conductivity of EG/graphene and water/graphene nanofluids were measured by transient hot wire method. Based on their observation, maximum improvement was about 64% at 50 °C when 0.056 vol % of functionalized 2D graphene was dispersed into deionized water. In another investigation, Wang et al. [36] experimentally inspected the influence of 2D graphene nanoparticles on thermophysical properties of ionic liquid [HMIM]BF₄ and demonstrated that 18.6% improvement in the thermal conductivity was attained at 65 °C with nanoparticle loading as low as of 0.06 wt % while no significant decrease in specific heat was observed. Unpredictably, viscosity of synthesized nanofluids was found to be lowered than base fluids which could be ascribed to the self-lubricating property of graphene. Apart from this, an opulent number of studies were also carried out with imidazolium ionic liquid based (IL) nanofluids [37,38], concluding that imidazolium based ILs can be employed as an excellent base fluids due to their salient features like non volatility, high thermal stability, and good interaction with carbon-based nanoparticles [39]. Plentiful studies are found in the literature that find numerous nanofluids improve the heat transport

efficiency of PV/T system [40–42]. Sardarabadi et al. [43] performed an experimental investigation to check the performance of a PV/T system using water/silica (SiO₂) nanofluids with two different concentrations of 1 wt % and 3 wt %. The overall energy efficiency and thermal efficiency of the PV/T collector increased by 7.9% and 12.8% using nanofluid of 3 wt %, while for 1% they were found to have increased by 3.6% and 7.6% than pure water. In another study, phase change material (PCM) along with ZnO/water nanofluid were used in a solar PV/T module as coolant medium to see the simultaneous effect experimentally [44]. To accomplish this, they designed two systems: one with phase change material PCM, PCM/(PV/T); and PV/T only. PCM/nanofluid based PV/T system was subjected to 13% increment in electrical efficiency compared to a typical PV/T system, while an almost 9% augmentation in thermal efficiency was also noticed together with more than 23% overall exergy efficiency enhancement. Recently, Abdallah et al. [41] studied a PV/T system with MWCNT (multi-wall carbon nanotube)/water nanofluids to investigate the electrical and thermal efficiency. The findings demonstrated that adding nanoparticles into the water had prompted the enhancement of the thermophysical properties of the working fluid which further increased the overall efficiency of the system. For different particles concentration ratio varying from 0 to 0.3 vol % of MWCNT, the analyzed results reported that nanofluids with 0.075 vol % of MWCNT exhibited the best performances, reducing the panel temperature by 12 °C that led 83.26% overall system efficiency at maximum incident radiation. In addition, Al₂O₃/water, TiO₂/water [45], Ag/water [42], sand-propylene glycol/water [46], and Fe₃O₄/water [47] were also explored to check their performance in PV/T systems in some studies. Reviewing the findings from literature, it can be attained that all relevant studies mainly focused on the optimization of solar PV/T systems using water-based nanofluid. Although overall thermal efficiency in some studies was satisfactory, they were only applicable at lower temperature ranges as water becomes thermally volatile at higher temperatures. Furthermore, variation in PV panel temperature and alteration of solar radiation were not studied in most cases. Therefore, it necessitates further studies with the aim of developing more promising nanofluids for solar PV/T system. MXene is a new family of 2D inorganic nanocomposite like graphene consisting of nano-sized layers of early transition metal carbides, carbonitrides, and nitrides [48]. MXene has a common formula of M_{n+1}X_nT_x ($n = 1, 2, \text{ and } 3$) which is synthesized from 3-D MAX phases [49] by selective etching of 'A' layer which is placed for a group IIIA or IVA element, M symbolizes early transition metal, T_x represents the surface termination (e.g., F, O, and OH) and X can be either carbon or nitrogen [50]. Since the surface termination/elemental composition is changeable [51], the properties of MXene can be altered rapidly, therefore rendering MXene more attractive than graphene. MXene has received immense research interest in numerous disciplines, such as nanomedicine, biosensors, electrochemical energy storage, and photothermal conversions [52–54]. In the present research, the authors formulate a novel ionanofluid with MXene and ionic liquid aqueous solution. The inclusion of 2D MXene into ionic liquid solutions has formulated a new class of ionanofluid. To the best of the authors' knowledge, this is the first time MXene dispersed ionanofluid has been formulated successfully and its heat transfer behavior on a hybrid PV/T has been investigated. It will certainly be helpful for researchers and guide them in further investigations with this novel nanomaterial in heat transfer applications. Thermal conductivity, specific heat capacity, density, and assessments for this novel IL+ water/MXene are studied for the first time to the best of the authors' knowledge. Thermal and electrical performance evaluation considering variable conditions (temperature, solar radiation) with this novel nanofluid in a hybrid PV/T solar system are new findings of this research work as well. Firstly, the authors formulate and characterize nanofluids and therefore, determine best concentration at which thermophysical properties are optimum. In consideration of their thermophysical properties, the authors favorably considered its possible application in hybrid PV/T system which could potentially serve as a more efficient alternative as heat transfer fluid for the application in hybrid PV/T solar system.

2. Materials, Methods, and Preparation

2.1. Materials

Ionic Liquid [MMIM][DMP] (1,3-Dimethylimidazolium dimethyl-phosphate) was supplied by Merck KGaA, Darmstadt, Germany. Table 1 represents the specifications of certificate analysis of [MMIM][DMP]. No further purification was accomplished during the sample preparation. Highly purified deionized water (Purity $\geq 99.998\%$) was prepared at nanomaterial research Centre of Sunway University, Malaysia.

Table 1. Properties of [MMIM][DMP].

Property	[MMIM][DMP]
Purity (HPLC)	$\geq 98.0\%$
Identity (NMR)	passed
Density	1.27 g/cm ³ (20 °C)
Water (KF)	$\leq 0.1\%$
Halides (IC)	$\leq 0.1\%$
Color	Yellow

2.2. Synthesis of MXene (Ti_3C_2)

In the synthesis of MXene ($Ti_3C_2T_x$), the following materials were used without any further purification: MAX Phase material (Ti_3AlC_2) from Y-Carbon Ltd., Ammonium hydrogen difluoride (reagent grade 95%, Sigma Aldrich, Kuala Lumpur, Malaysia) and sodium hydroxide (97% purity, pellets, Sigma Aldrich) were obtained. Firstly, a solution of 2M and NH_4HF_2 was prepared precisely as the main part of the wet chemistry etching process. Afterwards, the dilution process of the ammonium hydrogen difluoride was conducted using DI water to produce 20 ml of solution, followed by magnet-stirring at 300 rpm for 1 h and at room temperature using hot plate magnet stirrer (RCT BASIC, IKA, Staufen, Germany). 1 g of Ti_3AlC_2 was weighed using microbalance (Explorer series, EX224, Ohaus, Parsippany, NJ, USA), then added to the uniform well-prepared NH_4HF_2 solution. Adding the MAX phase material to the prepared solution was performed slowly as the reaction is exothermic. The MAX phase suspension in the NH_4HF_2 was magnet-stirred at 300 rpm for 48 h and room temperature continuously to conduct the etching process. After the etching process, a dilute solution of NaOH was poured until the pH of the suspension reached 6 and was filtered and rinsed several times with deionized water. The washing process was conducted using an ultrahigh centrifuge (Sorvall LYNX 6000, Thermo Scientific, Waltham, MA, USA) four times (10 m each times) at 3500 rpm. The achieved multilayered MXene (m- Ti_3C_2) was then sonicated for 1 h by means of ultrasonic probe sonicator ('FS-1200N') to obtain delaminated flakes of the MXene (d- Ti_3C_2). The synthesized delaminated flakes of MXene nanomaterial was dried in a vacuum oven (VO 500, MEMMERT Germany, Schwabach, Germany) overnight.

2.3. Preparation of Ionanofluid

The formulation of ionanofluid samples was accomplished by dispersion of Ti_3C_2 nanoparticles into IL aqueous solution precisely. To achieve this, IL aqueous solution was prepared by dissolving 20 vol % of [MMIM][DMP] into 80 vol % of deionized water by magnetic stirring for 30 m at 45 °C and 700 rpm to obtain a homogenous mixture. The viscosity of the ionic liquid is high; therefore, adding water contributes to reducing the viscosity of the solutions. Furthermore, strong hydrophilicity of MXene will offer better stability with adding water [55]. Firstly, Ti_3C_2 nanosheet was precisely weighted using an analytical microbalance (Ohaus, Model: Ex224, accuracy: 0.0001 g, Parsippany, NJ, USA) and directly added into the IL solutions at three different concentrations of 0.05, 0.10, and 0.20 wt %. Next, all sample solutions were stirred using hot plate magnetic stirrer (RCT basic IKAMAG® safety control, Staufen, Germany) for 1 h at 50 °C and 700 rpm. Finally, followed by an ultrasonic dispersion using a

1200 W, 20 kHz ultra sonicator (Ultrasonic Probe sonicator, Model: Fs-1200N, Hangzhou, China) for 30 m, a stable and well dispersed ionanofluid was formed by interrupting the hard agglomeration of MXene particles.

2.4. Characterization

The surface morphology of Ti_3C_2 nanosheet was inspected with a SEM (scanning electron microscopy) “Tescan, Model: Vega, Brno, Czech Republic”. The SEM device was operated at 15 kV voltage and 10 mA current to obtain accurate and sharp images. In order to inspect the layered structure of Ti_3C_2 , a sample area having significant number of layers was examined using SEM. Fourier transform infrared (FTIR) spectroscopy (Perkin Elmer®, Model: Spectrum Two™, Waltham, MA, USA) was employed to identify the chemical compositions and functional groups of the formulated nanofluids. The device was operated at a resolution of 4 cm^{-1} and each spectrum was obtained over 16 scans with a scan speed 0.2. The spectra were determined for infrared frequency region ranging from 400 to 4000 cm^{-1} . Quantitative absorbance of all samples was measured as a function of wavelength using a UV–vis spectrometer (Perkin Elmer®, Model: Lambda 750, Waltham, MA, USA)

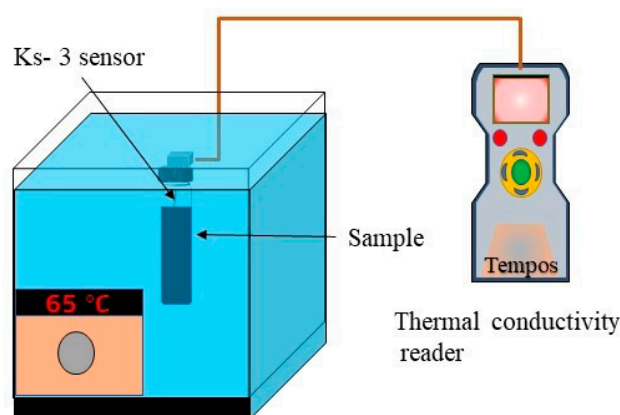
2.5. Thermophysical Properties Measurement

2.5.1. Thermal Conductivity

To assess the thermal conductivity, a transient hot wire method operated thermal property analyzer (Model: Tempos, Pullman, WA, USA) was employed affording an accuracy of $\pm 10\%$ for each sample. A 6 cm, Ks-3 sensor based single heated needle was employed to detect the temperature by dipping the needle into the sample inside a hot water bath. Before measuring the thermal conductivity, the device was calibrated precisely using pure glycerin at $20\text{ }^\circ\text{C}$. The calibration details are given in Table 2 and an illustration of the used setup is shown in Figure 1. Before taking each reading, the samples were equilibrated for at least 10 min as temperature reaches the anticipated value. The precision of measurement was confirmed by repeating each measurement for 5 times and taking the mean value of iterations.

Table 2. Calibration details of Tempos thermal conductivity analyzer.

Standard Sample	K_{measured}	$K_{\text{reference}}$ $\text{Wm}^{-1}\text{k}^{-1}$	Standard Deviation σ_k
Glycerin ($20\text{ }^\circ\text{C}$)	0.289	0.282	± 0.038



Constant Temperature water bath

Figure 1. Setup used for measuring thermal conductivity.

2.5.2. Specific Heat Capacity

In this study, the specific heat capacity (c_p) measurements of all samples were obtained using a (DSC). DSC-1000/C (Linseis, Germany), is a high resolution ($0.03 \mu\text{W}$) instrument and the measurements are conducted using an aluminum crucible of $40 \mu\text{L}$. The temperature ranges from $26 \text{ }^\circ\text{C}$ to $60 \text{ }^\circ\text{C}$ with the heating rate of $10 \text{ }^\circ\text{C}/\text{min}$. The synthesized samples are tightly sealed in a regular aluminum crucible with the capacity of $40 \mu\text{L}$ under a N_2 ambiance with a flow rate of $20 \text{ ml}/\text{min}$. The repeatability and calorimetric precision of temperature are $\pm 0.1 \text{ }^\circ\text{C}$ and $\pm 1\%$, respectively. Temperature and enthalpy calibrations for DSC are carried out employing four standard reference samples (indium, tin, lead, and zinc) provided by the supplier. One uniform protocol for c_p measurements of the nanofluid samples are adjusted to validate the precision of results. However, the measurement uncertainty ranged from 0.2% to a maximum 0.8% .

2.5.3. Measurement of Viscosity

A rheometer (Anton Paar, Model: MCR 92, Graz, Austria) was employed to measure the viscosity of the samples at a revolution rate of 100 rpm . Accuracy of the measurement was $\pm 1.0\%$ (in the range of -40 to $200 \text{ }^\circ\text{C}$ temperature) as stated by product specification. Viscosity of each sample was measured for the temperature range from $20 \text{ }^\circ\text{C}$ to $50 \text{ }^\circ\text{C}$.

2.5.4. Measurement of Density

A densitometer (Anton Paar, Density Meter, Model: DMATM1001, Graz, Austria) was employed to measure the temperature depended density. The densitometer was calibrated with air and pure distilled water by performing air test and water test respectively. The density of the sample was taken as a function of temperature from $20 \text{ }^\circ\text{C}$ to $60 \text{ }^\circ\text{C}$ with an accuracy of $0.0001 \text{ g}/\text{cm}^3$ and repeatability of $0.00005 \text{ g}/\text{cm}^3$.

2.5.5. Measurement of Thermal Stability

The thermogravimetric analysis (TGA) was performed to measure the thermal stability of each sample, showing the weight decomposition as a function of temperature. The analysis was performed with thermogravimetric analyzer (Perkin Elmer[®], Model: TGA 4000, Waltham, MA, USA). All the samples were heated from $30 \text{ }^\circ\text{C}$ to $500 \text{ }^\circ\text{C}$ in a compact ceramic furnace with a heating rate of $10 \text{ }^\circ\text{C}/\text{min}$ and a flow rate of $19.8 \text{ ml}/\text{min}$ of N_2 at 1.9 bar .

2.5.6. Measurement of Zeta Potential

Zeta potential is a common technique to measure the stability of nanofluids and colloidal solutions [56]. To assess the zeta potential measurement of the prepared ionanofluids at different concentrations, a particle analyzer (Litesizer-500, Anton paar, Graz, Austria) was employed. The measurements were repeated for at least three times for each sample.

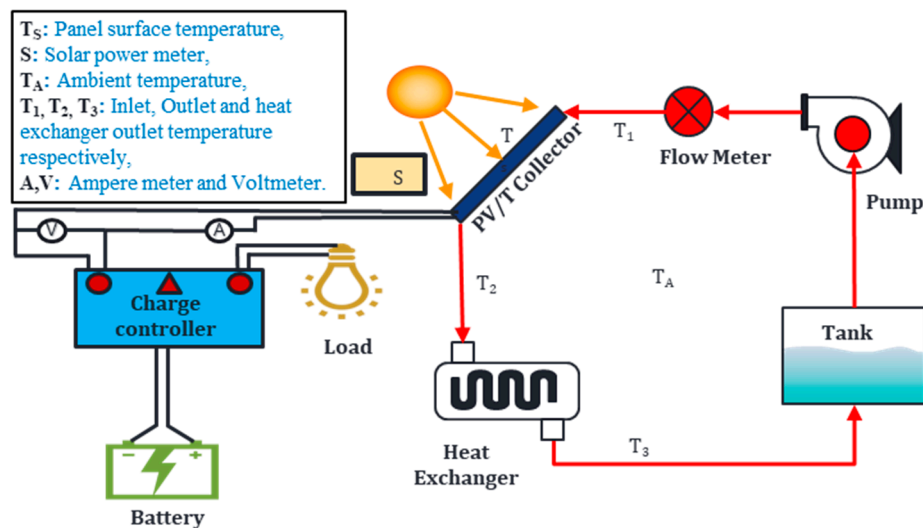
2.6. Physical Model of PV/T System

In a hybrid PV/Thermal system for controlling the temperature rise of PV module various active and passive techniques were employed by researchers. Many of them used nanofluid as a coolant at the back of the PV panel to lower the temperature, especially in hot arid climate for better electrical efficiency. The specification of PV panel used for simulation purpose in PV/thermal system is listed in Table 3.

Table 3. Specification of PV panel.

Make and Model No.	Vikram Solar, ELDORA VSP.72.AAA.03
Material	Polycrystalline Silicon Cell
Dimension	1955 × 982 × 36 mm
No. of cells	72
Peak power	300 W
Maximum Voltage (Vmpp)	37.05 V
Maximum Current (Impp)	8.10 A
Open circuit voltage (Voc)	45.58 V
Short circuit current (Isc)	8.58 A
Weight of PV module	20.5 Kg
Operating temperature range	−40 °C to +85 °C
Standard test condition (STC)	1000 W/m ² , AM 1.5, 25 °C

In this part, a numerical investigation is carried out to assess the performance of newly developed ionic liquid solution/MXene based nanofluid in PV/T system. The proposed work consists of hybrid PV/T system in which alumina/water, MXene/palm oil and IL+ water/MXene based nanofluid were employed and their performance are compared with water alone as a coolant numerically. A typical model of a PV/T system is presented in Figure 2, where the red color path indicates the thermal circuit and another one indicates the electrical circuit.



2.7. Numerical Modeling of PV/T Solar System

The problem under investigation comprises of PV module of 300 Watt which consist of four layers namely: PV solar cell, EVA (encapsulated vinyl acetate) on both sides of the solar cell, and a tedlar layer. Beneath the PV module, a heat exchanger in the form serpentine copper tubing is mounted (See Figure 3). The thicknesses of solar cell, EVA, and tedlar layers are 0.3 mm, 0.5 mm, and 0.1 mm respectively, remaining dimensions are the same as the PV panel i.e. (1955 mm × 982 mm). Finite element method-based Multiphysics software, COMSOL (Burlington, MA, USA) is used for numerical study. CFD and heat transfer modules of COMSOL are used to assess the performance parameters of PV/T system. It is assumed that the nanofluid flow is steady, three-dimensional, incompressible, and laminar. Transmissivity of EVA is about 100%, the role of dust on PV surface absorptivity is assumes negligible and temperature variation along the thickness of PV module assume to be zero. Furthermore, homogeneous mixture of nanoparticles in the base fluid is assumed (i.e., no particle agglomeration). In this study, [MMIM][DMP]+water/Ti₃C₂, palm oil/Ti₃C₂ based nanofluid with

0.2 wt % nanoparticle concentration are used as thermal conductivity is highest at this concentration. Thermal conductivity corresponds to 0.2 wt %, with different temperatures fitted to third order polynomial using regression analysis and inserted into a COMSOL environment using a user defined function. For alumina/water nanofluid, the Maxwell model is used for modelling thermal conductivity in which values of 0.611 W/m.K for water and 40 W/m.K for Al_2O_3 are used (see Equation (1)).

$$k_{nf} = k_{bf} \frac{k_s + 2k_{bf} - 2\phi(k_{bf} + k_s)}{k_s + k_{bf} + 2\phi(k_{bf} + k_s)} \quad (1)$$

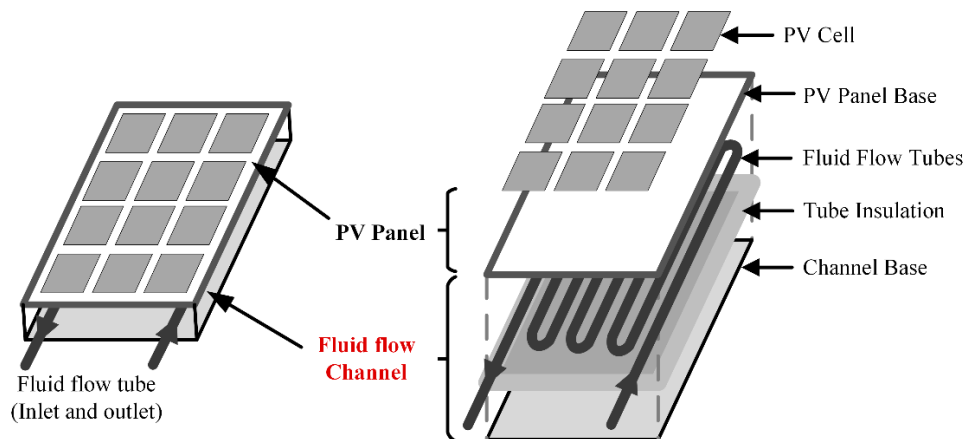


Figure 3. Schematic diagram of the proposed nanofluid backflow channel-based PV panel.

For modelling temperature dependent viscosity of IL+ water/MXene and palm oil/MXene nanofluids, regression analysis of experimental data is performed. For IL+ water/MXene nanofluid, thermophysical properties are experimentally obtained in present studies while previous experimental data has been used for palm oil/MXene nanofluids for same operation conditions [24]. The equation is incorporated into COMSOL using UDF (user defined function), as with thermal conductivity, and used for simulation purpose. For Al_2O_3 -water nanofluid Brinkman model is used for modelling viscosity. For solid domain in the PV/T system heat conduction equation is used to account for heat transfer. Thermal transport from PV panel surface to flow channel is solved by a heat conduction equation as shown below in Equations (2)–(4).

$$-\left(\frac{k}{\rho C_p}\right)\left(\frac{\partial^2 T}{\partial x^2} + \frac{\partial^2 T}{\partial y^2} + \frac{\partial^2 T}{\partial z^2}\right) = \alpha_p G - E_e - h_{panel-ted}(T_{penal} - T_{ted}) \quad (2)$$

The equation shows heat transfer from the PV panel to tedlar layer. Similarly, other thermal energy equations between other layers can be written in a similar fashion. Here α_p is the absorptivity of the panel, G is the irradiance, E_e is the electrical energy output, and $h_{panel-ted}$ is the heat transfer coefficient between panel and tedlar layer. Similarly, other heat transfer coefficients between the layers are defined in Equations (3) and (4). Values of these are adopted as constant and are listed in Table 4 as thermal and optical properties of PV/T system.

Table 4. Thermal and optical properties of PV/T system.

Properties	Values
Heat transfer coefficient from Panel to tedlar	150W/m ² K
Heat transfer coefficient from tedlar to tubing	77 W/m ² K
Heat transfer coefficient from tubing to nanofluid	66 W/m ² K
Absorptivity of PV module	0.9
Absorptivity of tedlar sheet	0.5
Emissivity of PV panel	0.99
Thermal conductivity of EVA	0.311 W/m·K
Thermal conductivity solar panel	148 W/m·K
Thermal conductivity of tedlar	0.15 W/m·K
Thermal conductivity of thermal paste	1.9 W/m·K
Thermal conductivity of tubes	2700 W/m·K

From the tedlar to serpentine tubing:

$$-\left(\frac{k}{\rho C_p}\right)\left(\frac{\partial^2 T}{\partial x^2} + \frac{\partial^2 T}{\partial y^2} + \frac{\partial^2 T}{\partial z^2}\right) = -h_{\text{penal-ted}}(T_p - T_{td}) - h_{\text{ted-tubing}}(T_{ted} - T_{tubing}) \quad (3)$$

From the serpentine tubing to nanofluid:

$$-\left(\frac{k}{\rho C_p}\right)\left(\frac{\partial^2 T}{\partial x^2} + \frac{\partial^2 T}{\partial y^2} + \frac{\partial^2 T}{\partial z^2}\right) = -h_{\text{ted-tubing}}(T_{ted} - T_{tubing}) - h_{\text{tubing-nf}}(T_{tubing} - T_{nf}) \quad (4)$$

The conjugate heat transfer equation is used for flow in the collector with both conduction and convection shown in Equation (5). Finally, the mass and momentum equation laminar fluid flow are given by Equations (6)–(9).

$$\rho_{nf} C_{Pnf} \left(u \frac{\partial T}{\partial x} + v \frac{\partial T}{\partial y} + w \frac{\partial T}{\partial z} \right) = K_{nf} \left(\frac{\partial^2 T}{\partial x^2} + \frac{\partial^2 T}{\partial y^2} + \frac{\partial^2 T}{\partial z^2} \right) \quad (5)$$

$$\frac{\partial u}{\partial x} + \frac{\partial v}{\partial y} + \frac{\partial w}{\partial z} = 0 \quad (6)$$

X-momentum:

$$\rho_{nf} \left(u \frac{\partial u}{\partial x} + v \frac{\partial u}{\partial y} + w \frac{\partial u}{\partial z} \right) = \frac{-\partial P}{\partial x} + \mu_{nf} \left(\frac{\partial^2 u}{\partial x^2} + \frac{\partial^2 u}{\partial y^2} + \frac{\partial^2 u}{\partial z^2} \right) \quad (7)$$

Y-momentum:

$$\rho_{nf} \left(u \frac{\partial v}{\partial x} + v \frac{\partial v}{\partial y} + w \frac{\partial v}{\partial z} \right) = \frac{-\partial P}{\partial y} + \mu_{nf} \left(\frac{\partial^2 v}{\partial x^2} + \frac{\partial^2 v}{\partial y^2} + \frac{\partial^2 v}{\partial z^2} \right) \quad (8)$$

Z-momentum:

$$\rho_{nf} \left(u \frac{\partial w}{\partial x} + v \frac{\partial w}{\partial y} + w \frac{\partial w}{\partial z} \right) = \frac{-\partial P}{\partial z} + \mu_{nf} \left(\frac{\partial^2 w}{\partial x^2} + \frac{\partial^2 w}{\partial y^2} + \frac{\partial^2 w}{\partial z^2} \right) \quad (9)$$

The density ρ_{nf} and heat capacitance, C_{Pnf} of nanofluid is assumed constant and their values were derived from empirical correlation available in archival literature [43] given below:

$$\rho_{nf} = (1 - \phi)\rho_{bf} + \phi\rho_s \quad (10)$$

$$C_{Pnf} = (1 - \phi)(C_p)_{bf} + \phi(C_p)_s \quad (11)$$

Energy balance is applied across the hybrid PV/T system given in Equation (12), which consists of irradiance coming from the sun, radiation from the panel surface, convection between PV/T system and ambient, thermal energy generated and the electrical power output.

$$G - P_{el} - P_{th} - Q'_{conv} - Q'_{rad} \quad (12)$$

Convective and radiative heat transfer from PV/T system are given by Equations (13) and (14) as follows. The convective heat transfer and radiative heat transfer from panel are calculated on the basis of Newton's law of cooling and Stefan–Boltzmann law respectively.

$$-n \cdot (-k\nabla T) = h_{total}(T_{surface} - T_{ambient}) \quad (13)$$

$$-n \cdot (-k\nabla T) = \varepsilon\sigma(T_{surface}^4 - T_{sky}^4) \quad (14)$$

where h_{total} is the total heat transfer coefficient evaluated as $h_{total} = (h_{forced}^3 + h_{natural}^3)^{\frac{1}{3}}$. This includes the both effect natural convection and forced convection over the panel. Where forced and natural convection heat transfer coefficient [46] are calculated by Equations (15) and (16).

$$h_{natural} = 1.78(T_{amb} + T_{surface})^{\frac{1}{3}} \quad (15)$$

$$h_{forced} = 2.8 + 3.0V_{wind} \quad (16)$$

Whereas the sky temperature is calculated using Swinbank relation [46] as $T_{sky} = 0.037536T_{amb}^4 + 0.32T_{amb}$. In Equation (14) ε is the emissivity of panel and σ is the Stefan–Boltzmann constant.

The electrical power and thermal energy output are expressed by

$$P_{el} = V_{oc} * I_{sc} * FF \quad (17)$$

$$P_{th} = mC_p(T_{out} - T_{in}) \quad (18)$$

Electrical and thermal efficiency are obtained by Equations (19) and (20), respectively

$$\eta_{el} = \frac{P_{el}}{G * A_c} \quad (19)$$

$$\eta_{th} = \frac{P_{th}}{G * A_c} \quad (20)$$

2.8. Boundary Conditions

Appropriate boundary conditions were employed across the domain as per the physics of problem. Across the top and bottom layer of PV module the boundary condition applied is $-n \cdot q = h_c(T_{amb} - T_s)$. Where \mathbf{n} is the surface normal and T_{amb} and T_s are the ambient temperature and surface temperature, respectively. For the fluid domain the inlet boundary condition is specified as velocity inlet along x -axis i.e., $u = U_o$, $v = 0$, $w = 0$ and $T = T_o$, for solid boundaries no-slip condition is used ($u = v = w = 0$), however at the outlet zero pressure boundary condition is used ($p = 0$). For solid–fluid interface heat flux continuity at the interface is used $(\frac{\partial T_s}{\partial n})_f = \frac{k_s}{k_f}(\frac{\partial T_s}{\partial n})_s$, adiabatic boundary condition is employed for the side surfaces of the system. Moreover, the lowermost plate of the hybrid solar PV/T system remains insulated.

2.9. Meshing and Grid Independence

The PV/T module was meshed in COMSOL Multiphysics® using the built-in physics-controlled mesh sequence setting shown in Figure 4. It consists of tetrahedral and triangular mesh element at

the sub-domain and at the boundary respectively. The number of mesh elements increase at each boundary so that the heat transfer and flow fields can be resolved accurately. For grid independence, simulation at 1000 W/m^2 and a mass flow rate of 0.05 kg/s is performed using water as a coolant with different mesh size (from coarser to finer) shown in Table 5. It was observed that there was no further change in panel temperature and outlet fluid temperature values after mesh no. 5. Thus, mesh no. 5 is chosen for simulation purposes. As far as quality measures are concerned, we checked the orthogonality, skewness, and growth rate of the elements and found satisfactory values of 0.65, 0.7, and 1.5 respectively. These values given us good quality mesh and the dialog box in COMSOL appears which states the minimum element quality to be 0.3319. If this value is $<10^{-4}$ the quality is extremely poor. Apart from this there is one more parameter termed as aspect ratio which is 0.3, and it is a thumb rule in COMSOL if it is greater than 0.1, it would not affect the quality of the solution, in this simulation mesh curvature factor is 0.3 and mesh curvature cut-off is 0.001. In the boundary layer meshing, 8 layers with a stretching factor of 1.2 and scaling factor of 1 is used. The initial layer thickness is designated as $1/50$ of the size of element on that boundary. The meshing along the thickness and around the tubing is shown in Figure 5a,b. The maximum and minimum deviation in the panel temperature for the six different meshes is 2.3% and 0.002% respectively. Similarly, for outlet fluid temperature, it is -2.94% and -0.22% . It was closely observed that, with consideration of mesh no. 6, the computational cost increases with meagre accuracy increment. Therefore, mesh no. 5 was considered for all the simulations.

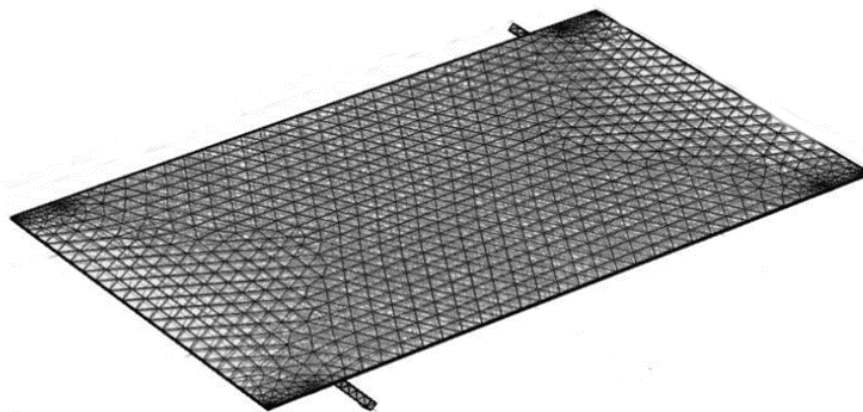


Figure 4. PV/T element with finite element meshing.

Table 5. Grid independence test.

S.No.	Mesh Size (no. of Elements)	Panel Temperature (°C)	% Deviation	Outlet Temperature (°C)	% Deviation	Time of Solution (s)
1	2.5×10^5	42.341	-	41.213	-	560
2	4×10^5	43.872	1.2%	40.751	-1.13%	720
3	6×10^5	44.003	0.29%	40.254	-1.23%	817
4	8×10^5	44.118	0.26%	39.104	-2.94%	1115
5	1.5×10^6	45.200	2.3%	38.889	-0.55%	1487
6	3.5×10^6	45.201	0.002%	38.801	-0.22%	1815

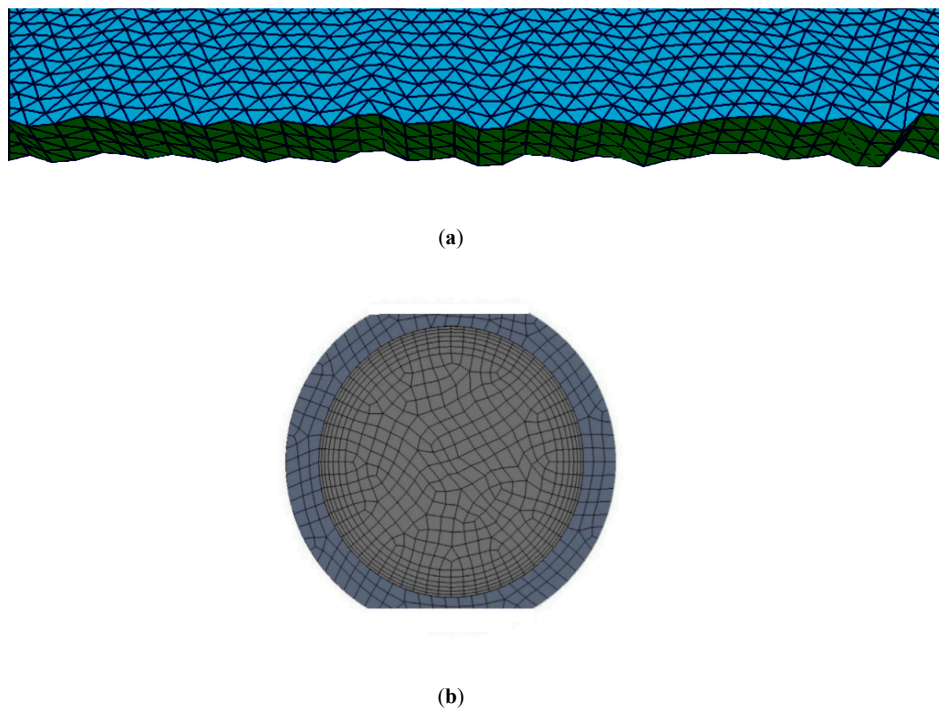


Figure 5. (a) Mesh along the thickness of panel. (b) Mesh inside and outside the tube.

3. Results and Discussions

3.1. Morphology and Characterization

Two-dimensional Ti_3C_2 was successfully synthesized from three-dimensional MAX (Ti_3AlC_2) phase which is evidenced by SEM micrographs presented in Figure 6a,b. The distinct self-staking layered structure of Ti_3C_2 which is clearly seen from SEM photographs is consistent with previous studies [57–59]. This layered structure is formed owing to the domino effect of van der Waals forces between two adjacent layers. Additionally, TEM images of multilayer flacks have a lateral size of up to 100 nanometers.

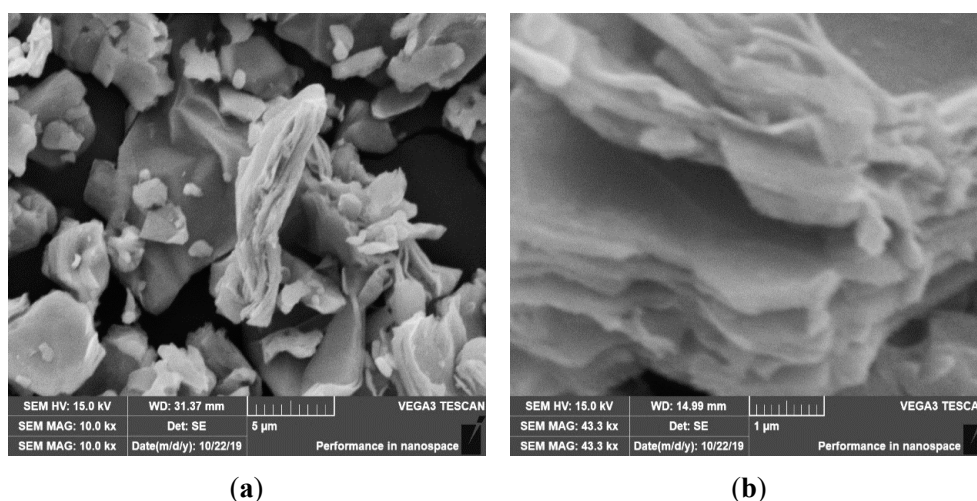


Figure 6. SEM micrographs of as synthesized Ti_3C_2 (MXene) (a) at 5 μm magnification (b) at 1 μm magnification.

The FTIR spectra of the formulated samples are presented in Figure 7. The broad peak appearing at wavelength 620 cm^{-1} is assigned to the chemically stable Ti–O bond, therefore, confirming the

dispersion of Ti_3C_2 (MXene) in the IL aqueous solutions which is in good agreement with previous studies [60,61]. Additionally, a few more peaks appearing in the spectra of the sample solutions indicates the presence of stretching vibration bands of O–H bond at 3337 cm^{-1} , C=N at 1643 cm^{-1} , C=C at 1579 cm^{-1} , C–O at 1176 cm^{-1} , C–N at 1037 cm^{-1} and bending vibration band C–H at 816 cm^{-1} . The assignment of these peaks strongly supports previous study in the literature for imidazolium-based ionic liquid [62]. The FTIR analysis implies that the dispersion of MXene into the IL solutions yields some functional groups which are stable, and no chemical reactions occur among the particles.

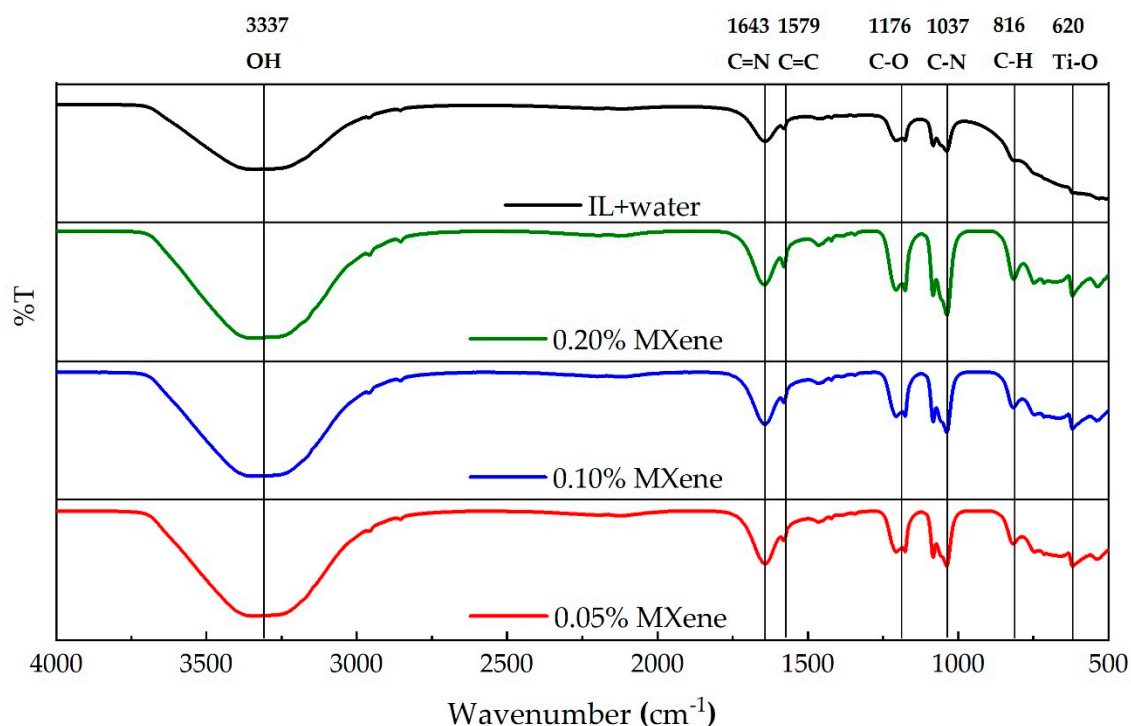


Figure 7. FTIR spectra of nanofluids at different concentrations.

Figure 8a,b illustrates the UV–vis spectra of pure IL solution and Ti_3C_2 dispersed ionanofluids at different wavelengths. As shown in the figure, the absorbance peak appearing at wavelength of 291 nm increases substantially with the addition of Ti_3C_2 nanosheets, demonstrating that the optical absorption capability of the solution increases notably with the addition of two dimensional Ti_3C_2 nanosheet. Similar trends were observed from past studies with carbon-based 2D nanomaterials [34,63]. Moreover, the linear relationship between the nano additives concentration and absorbance justifies the Beer's law fairly. This phenomenon is attributed to the high absorption ability of carbon and carbon-based nanocomposites. It must be noted that higher absorption ability of a fluid provides better performance for energy storage system specially for solar energy storage system [64].

Stability is substantially related to electro-kinetic potential differences between the stationary layer attached solid nanoparticles and dispersion medium [65]. A nanofluids must be stable enough before taking it for application. A nanofluid without stability will not be applicable even though it exhibits outstanding thermophysical and optical properties. The stability of [MMIM][DMP]+water/ Ti_3C_2 nanofluids were measured in terms of zeta (ζ) potential. Table 6 illustrates the values of ζ potential measured as a function of temperature. As shown from the table, the prepared ionanofluids exhibit good stability without adding any surfactants (a commonly practiced chemical treatment to improve the stability by promoting interactions among particles). This is due to the fact that, MXene is strongly hydrophilic in nature that have strong interactions with water solution [66]. Furthermore, IL [MMIM][DMP] is also hydrophilic which also contributed to improving stability [67]. On the other hand, ζ potential of the sample shows a trend to increase with increasing concentration from 0.05 wt %

to 0.10 wt % of Ti_3C_2 nanosheets. The increase in ζ potential can be explained by the fact that with increasing concentration the surface area of Ti_3C_2 nanosheet also increases, which in turn absorbs negative ions in their surface, therefore, the potential difference between the Ti_3C_2 surface and IL solutions increases. However, further increase in Ti_3C_2 concentration causes a decline in the ζ potential. A possible explanation for this is that although the surface area of the nanoparticles is increased, correspondingly the attractive forces between them are also increased causing their zeta potential to deteriorate. Similar trends were noticed in previous findings [68,69]. The effect of temperature on zeta potential value is also significant. For each case the ζ potential value increases significantly with increasing temperature which exhibits more stable structure with liquid particles. This is possibly due to the reduction of intermolecular forces between Ti_3C_2 particles as the Brownian motion increased with the temperature. Similar observations were also noticed for 2D graphene and carbon-based nanosheets in water solution [70]. As the ζ potential value increases with temperature, it clearly indicates the dispersion stability is improved at higher temperatures, which can be an advantage for better performance at higher temperatures. Taken together, these results suggest that a critical concentration is required to obtain the optimum value of the ζ potential which assures better stability of the suspension solution.

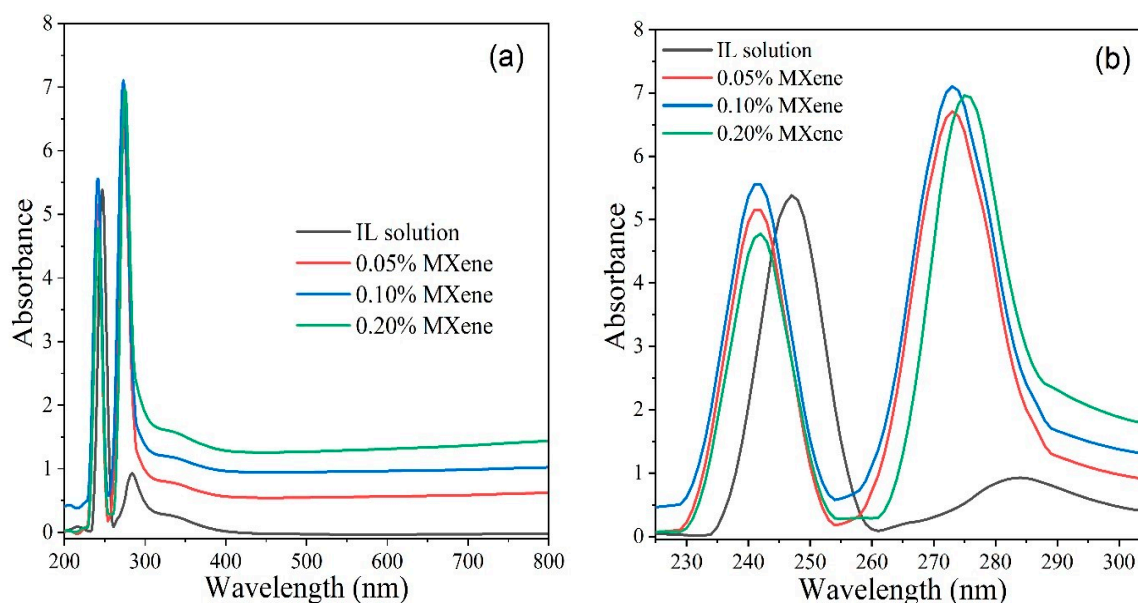


Figure 8. (a) UV-vis spectra of pure IL solution and nanofluids, (b) magnified view from 225 nm to 305 nm wavelength.

Table 6. ζ -potential of ionanofluids different weight concentration Ti_3C_2 .

Concentration	Zeta Potential (mV)					
	25 °C	Uncertainty (%)	45 °C	Uncertainty (%)	60 °C	Uncertainty (%)
0.05	-18.33	<5	-29.52	<5	-38.68	<5
0.10	-19.16	<5	-34.64	<5	-39.54	<5
0.20	-17.88	<5	-32.15	<5	-35.35	<5

3.2. Thermophysical Properties

3.2.1. Thermal Conductivity

The thermal conductivities of the IL+ water solution and $[\text{MMIM}][\text{DMP}]+\text{water}/\text{Ti}_3\text{C}_2$ ionanofluids was determined at four distinct temperatures, ranging from 25 °C to 60 °C. The obtained values of

each sample are depicted in Figure 9a and thermal conductivity enhancement of the ionanofluids ($K_{nf}/K_{IL}-1$) are shown in Figure 9b. As shown in Figure 9a, thermal conductivity of IL aqueous solution at 25 °C is 0.468 W/m.K and rises up to 0.597 W/m.K as the temperature reaches 60 °C which completely agrees with the previous study at the same volume fraction and temperature of IL [71]. The trend of the thermal conductivity shows significant improvement with the addition of Ti_3C_2 nanosheets are into [MMIM][DMP]+water solution and continues improving as the loading of Ti_3C_2 nanosheets are increases. High surface area of nanoparticles, better heat transport properties, and good interaction with fluid nanoparticles are the primary facotrs that improve thermal conductivity. In addition, thermal conductivity of all samples increases remarkably with increasing temperature as a consequence of intensified Brownian motion of liquid molecules. As seen from Figure 9b, a maximum 47% enhancement in thermal conductivity occurs at 35 °C for 0.20% loading of Ti_3C_2 nanosheets, which is higher compared to 4.95% with graphene nanosheet/water nanofluids [72], 22.9% with graphene/[HMIM][BF₄] ionanofluid [73], and 2% with GNP/EG nanofluids [74]. As higher thermal conductivity of HTFs offers higher thermal efficiency, it can be asserted that MXene dispersed nanofluid can be employed as novel HTF for solar PV/T systems.

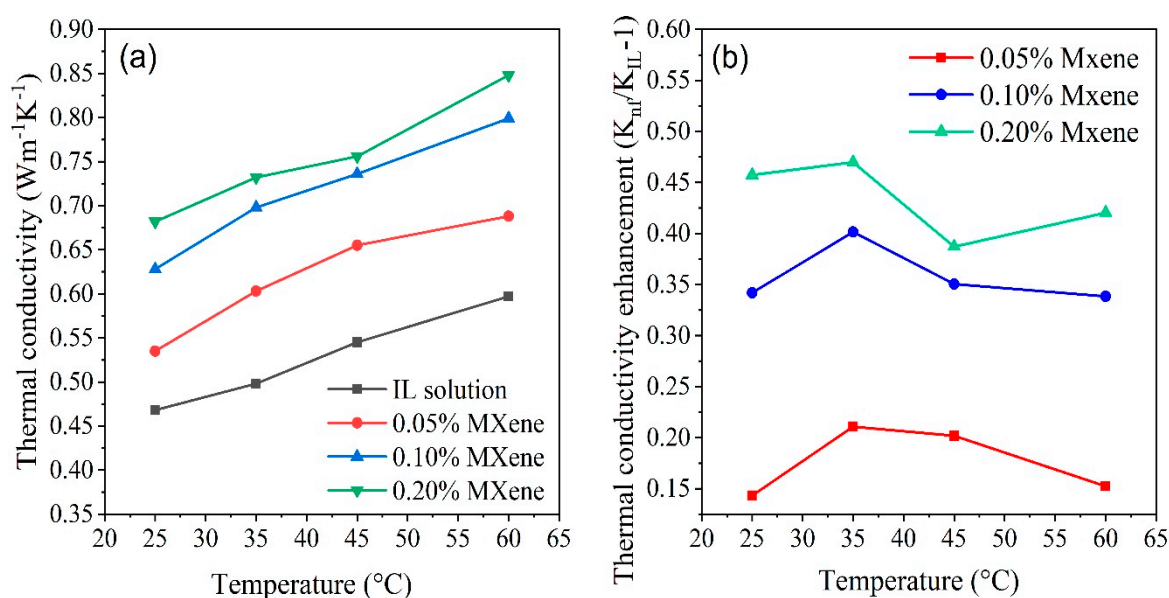


Figure 9. (a) Experimental values of thermal conductivity at different concentrations of Ti_3C_2 nanosheets for varying temperatures. (b) Thermal conductivity enhancement ratio at different temperatures with respect to IL+ water solution.

3.2.2. Specific Heat

The specific heat of [MMIM][DMP]+water solution and [MMIM][DMP]+water/ Ti_3C_2 nanofluids for 0.05, 0.10, and 0.20 wt % of nanoparticle loading were measured in the temperature ranges from 26 °C to 60 °C. Figure 10 elucidates the variation of specific heat for base fluid and ionanofluids as a function of temperature. According to the trend lines, it is obvious that the dispersion of Ti_3C_2 nanosheets into the IL+ water solution causes the increase of specific heat of the solution which could be ascribed to the high specific surface energy of 2D Ti_3C_2 nanosheets. Similar trends were noticed from previous studies for ternary carbonate/CNT nanofluids [75], molten salt/SiO₂ [76]. Furthermore, the specific heat is found to rise with increasing temperature for each sample. In other words, as the fluid heats up, the kinetic energy increases causing the fluid molecules to reach vibration state which enhances energy storage ability. Previous studies [36,77] showed similar trends which are consistent with the present study and mostly for imidazolium-based ionanofluids [78]. The specific heat of pure [MMIM][DMP]+water solution rises from 2.141 to 2.222 J/g.K with increasing temperature from 26 °C to 60 °C while for 0.05, 0.10, and 0.20 wt % of Ti_3C_2 ionanofluids, specific heat is noticed to increase

linearly from 2.271 to 2.344 J/g.K, 2.315 to 2.397 J/g.K, and 2.399 to 2.537, J/g.K respectively for the same temperature enhancement. It must be noted that enhanced specific heat would result in a better outcome for solar thermal application, especially for energy storage systems.

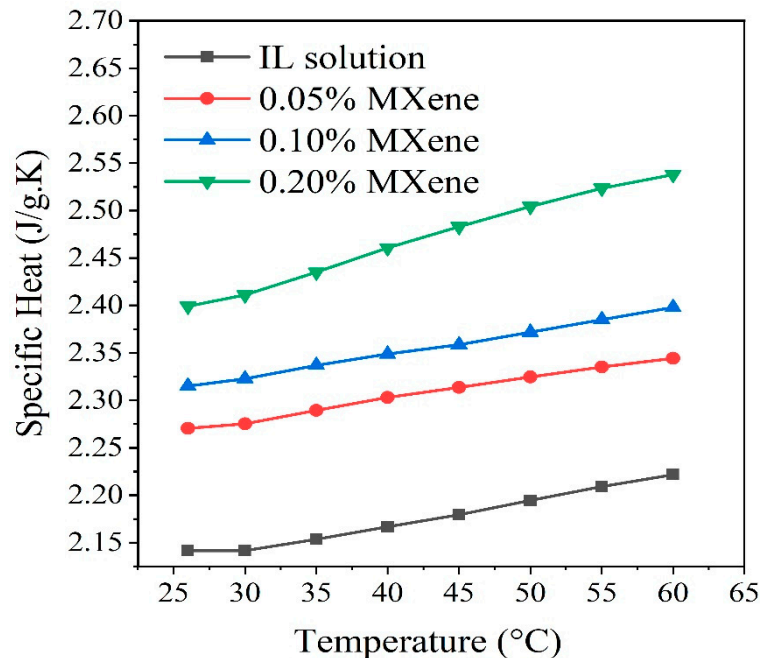


Figure 10. Specific heat capacity of IL aqueous solution and ionanofluids with various concentrations of Ti_3C_2 .

3.2.3. Viscosity

Figure 11 illustrates the variation of dynamic viscosity of pure IL+water solutions and its nanofluids for different concentrations of Ti_3C_2 nanosheet in the temperature range from 25 °C to 60 °C. The viscosity of the pure IL+ water is lower than that of pure IL as less viscous water is added to IL [79]. It is obvious from the graph that the dynamic viscosity of the IL+ water solution increases from 2.694 mPa.s to 2.986 mPa.s when Ti_3C_2 nanosheets are added by 0.05 wt % while for 0.10 wt % and 0.20 wt % nanofluids, the viscosity further increases to 3.011 mPa.s and 3.066 mPa.s respectively. On the contrary, viscosity is noticed to decrease significantly as the temperature rises which complies with previous results [80,81]. The increase in viscosity of nanofluids attributes to the increasing shear stress with addition of Ti_3C_2 nanosheets into the IL+ water solutions. In other words, increasing the temperature weakens the intermolecular forces between the Ti_3C_2 particles and the solution itself. Hence, viscosity decreases as the temperature rises. However, lower viscosity is one of the major considerations for the application of HTF as higher viscosity increases pressure drop, therefore, it requires higher pumping power. In the current study, the increase in viscosity is almost negligible with increasing Ti_3C_2 nanosheet loading. Therefore, this conspicuous result emphasizes the reliability of using nanofluids in solar PV/T systems as a novel HTF.

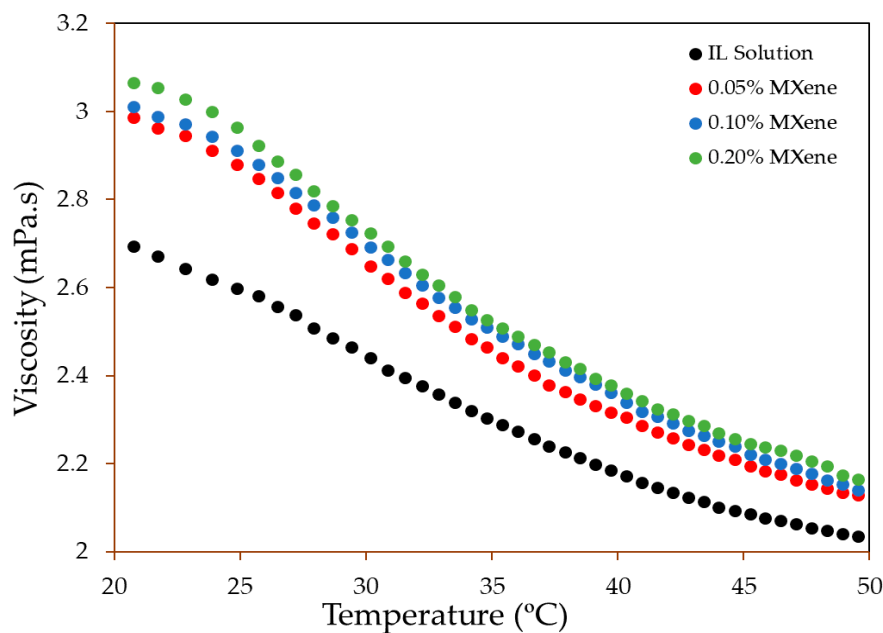


Figure 11. Dynamic viscosity of IL aqueous solution and ionanofluids with various concentration of Ti_3C_2 .

3.2.4. Density

Density is also an important parameter for heat transfer systems as the pressure drop and pumping power significantly depend on density of the working fluids. Figure 12 illustrates the experimental density variation of the IL solution and ionanofluid at concentrations of 0.05, 0.10, and 0.20 wt % of Ti_3C_2 nanosheets. The result indicates a small increment of density when Ti_3C_2 nanosheets are dispersed into the IL solution at different concentrations which attributes to the addition of a high-density nanocomposites into the base fluid. In addition, the density decreases with increasing temperature as the kinetic energy of the fluids improves. In this study, maximum density occurs for the concentration of 0.20 wt % of Ti_3C_2 as expected as it rises from 1.037 gm/cm^3 to 1.053 gm/cm^3 at $20 \text{ }^\circ\text{C}$. Since enhancement is lower than 2%, its effect the performance of the solar PV/T system will be negligible.

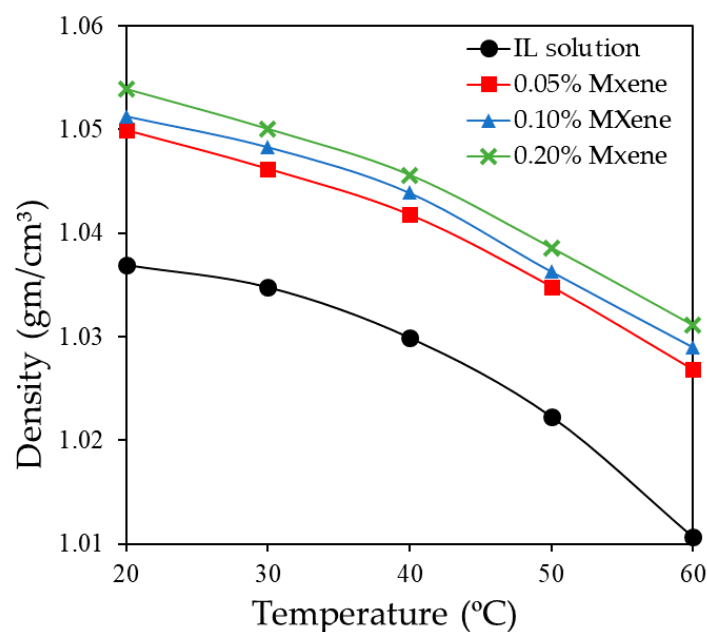


Figure 12. Density curve of IL+ water and IL + water/ Ti_3C_2 .

3.2.5. Thermal Stability

Thermal stability is another important parameter of thermal fluids since the applicability of thermal fluids greatly depended on their mass decomposition rate at working temperature [82]. The thermal stability is assessed by performing thermo gravimetric analysis (TGA) for each sample. Figure 13 illustrates the decomposition rate of the samples in terms of temperature. It is evident from the graph that all the samples are appreciably stable at up to 45 °C while initial decomposition of water starts at 45 °C for each sample. However, water contents are totally decomposed within 90 °C to 120 °C for different samples. It is obvious that the decomposition temperature of the nanofluids increases by dispersing Ti_3C_2 particles into the IL solution. This is attributed to the fact that some hydroxyl groups are introduced on the surface layers of the Ti_3C_2 particles that forms new functional groups containing high thermal stability. Furthermore, in the case of existing IL contents, no weight decomposes at up to 250 °C demonstrating all chemical bonds existing in the IL are strongly stable at up to 250 °C. Above 250 °C, all samples begin to decompose again and continue until all ionic liquids are fully decomposed nearly at 500 °C. The TGA curves demonstrate that the existence of Ti_3C_2 nanosheets in IL solutions does not lead to significant alteration in the decomposition rate of the IL solutions.

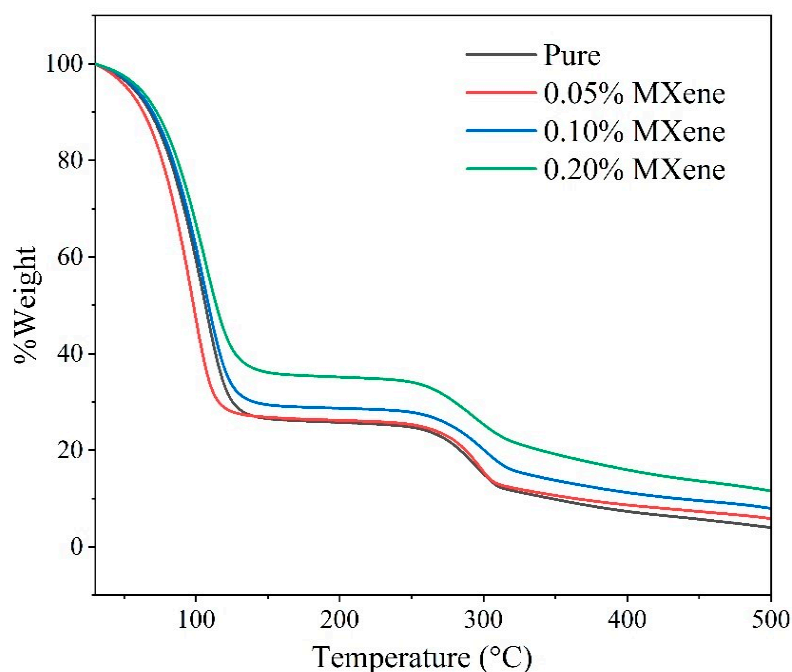


Figure 13. TGA curve of the IL+ water solution and ionanofluids at different concentrations of Ti_3C_2 .

3.3. Validation of Numerical Model

A validation of model with previous results is depicted in Table 7. For validation purposes, a comparison is made with alumina-water nanofluid with numerical as well as experimental study of Sardarbadhi et al. [83] and Lee et al. [84], respectively. It was observed that the results are in good agreement with previous results and shows an error of about 0.25% for panel temperature with numerical study and for electrical efficiency around 0.05% with experimental study.

Table 7. Code validation of PV panel surface temperature and electrical efficiency.

Panel temperature (°C)		Percentage Error	Remark
Present Research	Sardarabadi et al. [83]		
56.35	56.21	0.25%	At 1000 W/m ² and at a flow rate of 0.025kg/s (Numerical study of [83])
Electrical efficiency			
Present research	Lee et al. [84]		
12.15	12.22	0.5%	At 1000 W/m ² and at a flow rate of 0.05kg/s (Experimental study of [84])

3.4. Performance of Solar PV/T System

To maintain the PV module temperature in the permissible limit, three different coolants were examined in this study. All the simulations were carried out at 1000 W/m² with nanoparticle concentration of 0.2 wt %. Figure 14a shows comparison with water, water/Al₂O₃, palm oil/MXene, and the newly developed IL+ water/MXene nanofluid to identify the effect on PV panel temperature during the daytime from 9:00 a.m. to 17:00 p.m. The simulation is scattered at different times, alternatively we can say at different irradiance levels, and the average PV module temperature was noted for particular times or irradiances. Next, we plotted the curve for all times and joined them smoothly. It is not a transient situation. It was observed that MXene/IL+water solution shows a larger temperature drop across the PV panel, hence exhibiting better thermal performance. It is obvious from the figure that, at around 1:30 pm, the difference in the temperature between PV/T system using alumina nanofluid and the PV/T system using IL+water/MXene is 7.9 °C—i.e. IL+water/MXene nanofluids—showed a 15.19% increment in the heat removal performance relative to alumina based nanofluid and around 8.5% increment in the heat removal performance relative to palm oil/MXene nanofluid. This behavior is attributed to higher thermal conductivity of MXene nanoparticles as well as ionic liquid in comparison to palm oil as a base fluid.

Figure 14b presented the comparison of electrical efficiency with varying mass flow rate for three coolants as mentioned above. The electrical efficiency is enhanced with increasing flow rate, for instance, using IL+water/MXene and palm oil/MXene nanofluids, efficiency increases from 12.2% to 13.95% and 12.2% to 13.15% respectively when mass flow rate increases from 0.01 kg/s to 0.07 kg/s. Hence, by using palm oil based nanofluid in the hybrid PV/T system, a 7.8% electrical efficiency improvement is achieved in comparison to alumina nanofluid at 0.07 kg/s mass flow rate. Furthermore, by employing IL+water/MXene and at 0.07 kg/s mass flow rate, an electrical efficiency improvement of 14.4% is achieved in comparison to alumina/water nanofluid.

In Figure 14c, thermal efficiency variation with mass flow rate is depicted for different coolants. It is evident from the figure that higher mass flow rate offers better thermal efficiency of the PV/T system irrespective of type of coolant. At a maximum mass flow rate of 0.07 kg/s, water shows 63.3% thermal efficiency, meanwhile alumina/water shows 71.18% thermal efficiency, MXene/palm oil shows 79.13% thermal efficiency, and IL+ water/MXene shows 81.15% thermal efficiency. It is clear from the results that IL solution based nanofluid is performing better than that of palm oil and water based nanofluids and has high heat transfer capability. IL+water/MXene has increased the thermal efficiency by 14% in comparison to alumina/water nanofluid.

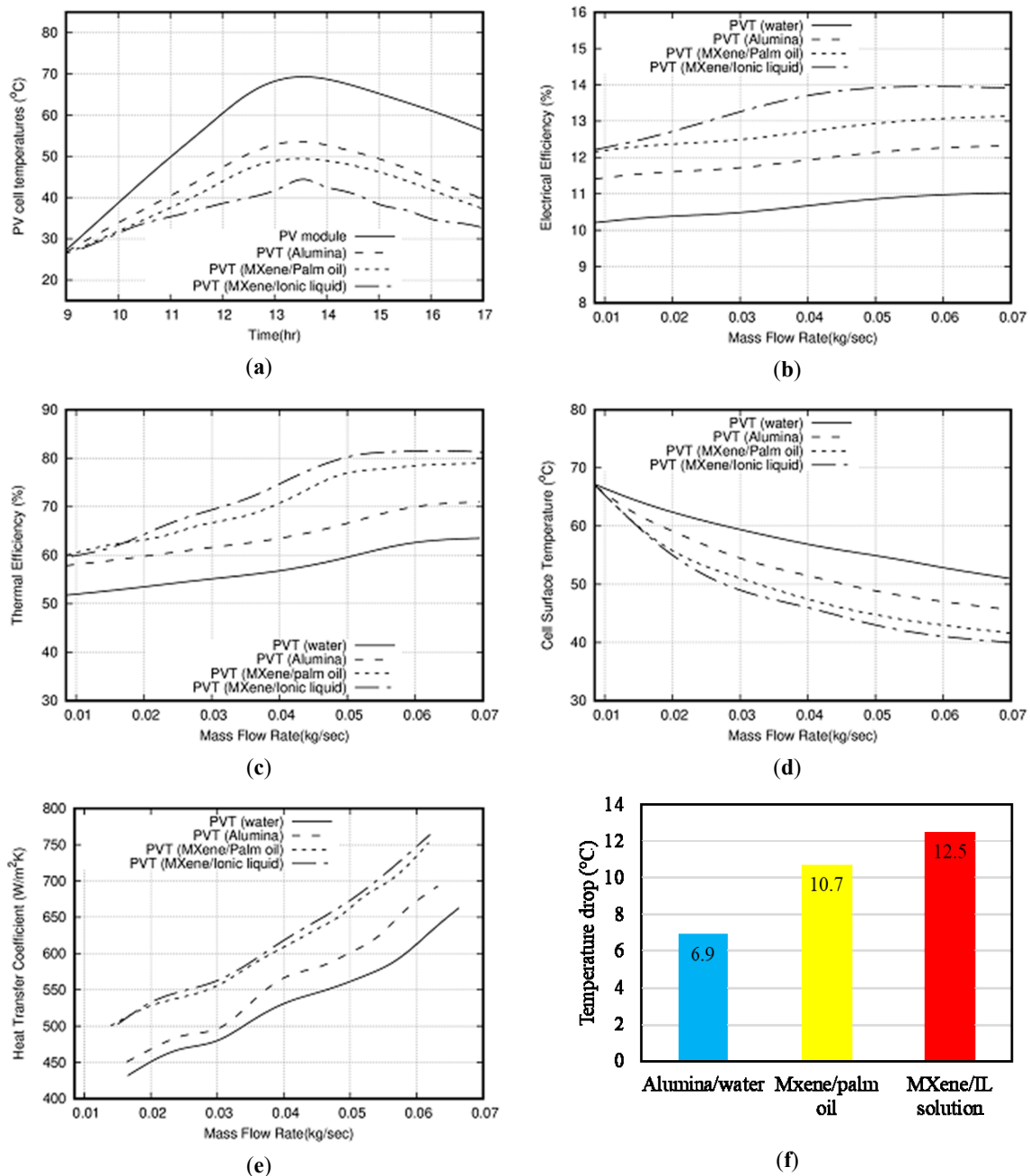


Figure 14. (a) Variation of PV panel temperature with time during a day for different types of coolant. (b) Electrical efficiency of PV/T system as a function of mass flow rate with different types of coolant. (c) Thermal efficiency of PV/T system as a function of mass flow rate with different types of coolant. (d) PV panel temperature as a function of mass flow rate using different types of coolant. (e) PV/T system heat transfer coefficient variation with mass flow rate using different types of coolant. (f) Drop in PV panel temperature by using different nanofluid types in comparison to a water-cooled system.

Figure 14d presents the PV panel temperature with mass flow rate. It is obvious from the graph that the initial range of mass flow rate is less than 0.015kg/s and there is not much variation in the PV surface temperature. However, a decreasing trend is observed with significant variation thereafter. This is due to the increased convection rate from the module which decreases the panel surface temperature with increases in mass flow rate. At a maximum flow rate of 0.07 kg/s, the temperatures of the PV surface with alumina/water, palm oil/MXene, and IL+ water/MXene nanofluids are 45.07, 42.5, and 40.5 °C respectively.

Finally, the heat transfer coefficient variation with mass flow rate is shown in Figure 14e. It was observed from the plot that heat transfer coefficient follows the increasing trend with mass flow rate irrespective of fluid used in the present study. Maximum percentage enhancement of 12.6% is achieved at 0.06 kg/s for IL+ water/MXene relative to the Al_2O_3 /water nanofluid. Additionally, 2% enhancement is accomplished at 0.06 kg/s for IL +water/MXene relative to palm oil/MXene nanofluid. Figure 14f shows the temperature drop using three types of nanofluid in PV/T systems which is relative to water coolant PV/T system. The maximum temperature drop of 12.5 °C is achieved using IL+water/MXene as a coolant at maximum mass flow rate. It is clear from the results that IL+water/MXene is showing outstanding results in terms of thermal and electrical performance with its counterpart palm oil/MXene and alumina nanofluid.

4. Conclusions

In this present work, IL+ water nanofluids are formulated with novel 2D MXene (Ti_3C_2) nanosheet at three different concentrations (0.05, 0.10, and 0.20 wt %) and their thermophysical properties (thermal conductivity, viscosity specific heat, density, and TGA) and optical properties (SEM, FTIR, UV-vis) are measured. On the basis of their optical and thermophysical properties, authors were highly motivated to apply this synthesized nanofluids in solar cooling system. As a consequence, a simulation-based application is performed with synthesized ionanofluid along with two other nanofluids (water/alumina, olein palm oil/MXene) in a hybrid solar PV/T system to compare their thermal performances. The findings of the investigation can be concluded as follows:

- The 2D MXene were successfully synthesized from 3D MAX phase and SEM analyses were performed to inspect the morphology of MXene before formulating ionanofluids.
- The formulated ionanofluids showed good stability without adding any surfactants or chemical treatment. Optical property measurement also showed a significant improvement in absorbance (UV-vis analysis) capability which may be considered a promising aspect of solar energy storage systems. The FTIR analyses also showed that the MXene particles were well dispersed into the solution and they were chemically stable.
- Superior results were also obtained for thermophysical properties as the thermal conductivity enhancements are significant at each concentration of MXene; however, a maximum of 47% enhancement is noticed at 0.2 wt %. In addition, thermal conductivity increases substantially as the temperature rises from 20 °C to 60 °C.
- Interestingly, viscosity is found to be decreased by adding MXene nanosheets which might be attributed to their self-lubricating property. Specific heat increases with both increasing temperature and concentration while density is found to increase with concentration but decrease as temperature increases. TGA analysis also confirms that no significant decomposition occurs up to 60 °C within the samples.
- A simulation-based study has been conducted with IL+ water/MXene in a PV/T system along with two other nanofluids (water/alumina and palm oil/MXene) to assess the performance. IL+ water/MXene nanofluid with 20 wt % concentrations exhibits highest electrical efficiency, overall thermal efficiency, and heat transfer coefficient in comparison with water, Al_3O_3 /water, and palm oil/MXene. Thermal efficiency of the considered PV/T system increases from 12.2 to 13.95% as flow rate increases from 0.01 to 0.07 kg/s with IL+ water/MXene. Moreover, thermal efficiency is also increased by 81.15% while, heat transfer coefficient is also increased by 12.6% and 2% for IL+ water/MXene compared to water/alumina and palm oil/MXene.

Author Contributions: L.D.: Conceptions of work, research, draft preparing, writing. K.H.: Research, draft editing, analyzing, R.S.: writing—directing, editing, and reviewing. N.A., S.M.Y., and F.R.: simulation and analysis. All authors have read and agreed to the published version of the manuscript.

Funding: This research was funded by Sunway University, grant number- STR-RCTRRCNMET-001-2019 and APC was funded by Yayasan Universiti Teknologi PETRONAS, Grant number- 015LC0-118.

Acknowledgments: The authors gratefully acknowledge Sunway University and Universiti Teknologi Petronas, Malaysia and Sunway University, Malaysia for mutual research collaboration. Deepest appreciation also goes to RCNMET, Sunway University for financial support (project no. STR-RCTRRCNMET-001-2019).

Conflicts of Interest: The authors declare no conflict of interest.

Nomenclature

Nomenclature		σ	Stefan Boltzmann Constant, $W/(m^2.K^4)$
A_c	area of collector (m^2)	<i>Subscripts</i>	
c_p	Specific heat (J/K)	<i>amb</i>	ambient
FF	field factor	<i>el</i>	electrical
G	solar radiation intensity (W/m^2)	<i>bf</i>	base fluid
H	convective heat transfer coefficient ($W/m^2.K$)	<i>in</i>	inlet
I_{sc}	short circuit current (A)	<i>out</i>	outlet
k_{nf}	thermal conductivity of nanofluid ($W/m.K$)	<i>s</i>	solid particle
k_{bf}	thermal conductivity of base fluid ($W/m.K$)	<i>th</i>	thermal
k_s	thermal conductivity of nanoparticle ($W/m.K$)	<i>nf</i>	Nanofluids
Q'_{conv}	heat transfer due to convection (W)	<i>Abbreviations</i>	
P_{th}	thermal power output (W)	FTIR	Fourier-transform infrared spectroscopy
P_{el}	electrical power output (W)	NMR	nuclear magnetic resonance
Q'_{rad}	heat loss due to radiation (W)	IC	ion chromatographic
T	temperature (K)	KF	Karl Fischer
V_{oc}	open circuit voltage (V)	IL	ionic liquid
<i>Greeks</i>		HPLC	high performance liquid chromatography
ζ	zeta potential, mV	TGA	thermogravimetric analysis
Φ	nanoparticle weight fraction	SEM	scanning electron microscopy
ρ	density, kg/m^3	PV/T	photovoltaic thermal
η	efficiency	SEM	scanning electron microscopy
ε	emissivity	UV-vis	ultraviolet-visible spectroscopy
		UDF	user defined function

References

- IEA. World Energy Outlook 2019. 2019. Available online: <https://www.iea.org/reports/world-energy-outlook-2019> (accessed on 26 February 2020).
- Krishna, Y.; Faizal, M.; Saidur, R.; Ng, K.C.; Aslfattahi, N. State-of-the-art heat transfer fluids for parabolic trough collector. *Int. J. Heat Mass Transf.* **2020**, *152*, 119541. [CrossRef]
- Aslfattahi, N.; Saidur, R.; Sidik, N.A.C.; Sabri, M.F.M.; Zahir, M.H. Experimental Assessment of a Novel Eutectic Binary Molten Salt-based Hexagonal Boron Nitride Nanocomposite as a Promising PCM with Enhanced Specific Heat Capacity. *J. Adv. Res. Fluid Mech. Therm. Sci.* **2020**, 73–85. [CrossRef]
- Moghim Ardekani, M. *Optical Thermal and Economic Optimisation of a Linear Fresnel Collector*; University of Pretoria: Pretoria, South Africa, 2017.
- Yang, M.; Wang, S.; Zhu, Y.; Taylor, R.A.; Moghim, M.; Wang, Y.J.E. Thermal Stability and Performance Testing of Oil-based CuO Nanofluids for Solar Thermal Applications. *Energies* **2020**, *13*, 876. [CrossRef]
- Thirugnanasambandam, M.; Iniyar, S.; Goic, R. A review of solar thermal technologies. *Renew. Sustain. Energy Rev.* **2010**, *14*, 312–322. [CrossRef]
- Borode, A.; Ahmed, N.; Olubambi, P. A review of solar collectors using carbon-based nanofluids. *J. Clean. Prod.* **2019**, *241*, 118311. [CrossRef]
- Hjerrild, N.E.; Mesgari, S.; Crisostomo, F.; Scott, J.A.; Amal, R.; Taylor, R.A. Hybrid PV/T enhancement using selectively absorbing Ag-SiO₂/carbon nanofluids. *Sol. Energy Mater. Sol. Cells* **2016**, *147*, 281–287. [CrossRef]

9. Aguilar, T.; Sani, E.; Mercatelli, L.; Carrillo-Berdugo, I.; Torres, E.; Navas, J. Exfoliated graphene oxide-based nanofluids with enhanced thermal and optical properties for solar collectors in concentrating solar power. *J. Mol. Liq.* **2020**, *306*, 112862. [[CrossRef](#)]
10. Sadeghzadeh, M.; Maddah, H.; Ahmadi, M.H.; Khadang, A.; Ghazvini, M.; Mosavi, A.; Nabipour, N. Prediction of Thermo-Physical Properties of TiO₂-Al₂O₃/Water Nanoparticles by Using Artificial Neural Network. *Nanomaterials* **2020**, *10*, 697. [[CrossRef](#)]
11. Abdelrazik, A.; Tan, K.; Aslfattahi, N.; Arifutzzaman, A.; Saidur, R.; Al-Sulaiman, F.J.S.E. Optical, stability and energy performance of water-based MXene nanofluids in hybrid PV/thermal solar systems. *Sol. Energy* **2020**, *204*, 32–47. [[CrossRef](#)]
12. Zhu, D.; Wang, L.; Yu, W.; Xie, H. Intriguingly high thermal conductivity increment for CuO nanowires contained nanofluids with low viscosity. *Sci. Rep.* **2018**, *8*, 5282. [[CrossRef](#)] [[PubMed](#)]
13. Li, X.; Zeng, G.; Lei, X. The stability, optical properties and solar-thermal conversion performance of SiC-MWCNTs hybrid nanofluids for the direct absorption solar collector (DASC) application. *Sol. Energy Mater. Sol. Cells* **2019**, *206*, 110323. [[CrossRef](#)]
14. Sang, L.; Ai, W.; Wu, Y.; Ma, C. SiO₂-ternary carbonate nanofluids prepared by mechanical mixing at high temperature: Enhanced specific heat capacity and thermal conductivity. *Sol. Energy Mater. Sol. Cells* **2019**, *203*, 110193. [[CrossRef](#)]
15. Bakthavatchalam, B.; Habib, K.; Saidur, R.; Saha, B.B.; Irshad, K. Comprehensive study on nanofluid and ionanofluid for heat transfer enhancement: A review on current and future perspective. *J. Mol. Liq.* **2020**, *305*, 112787. [[CrossRef](#)]
16. Aslfattahi, N.; Samyilingam, L.; Abdelrazik, A.; Arifutzzaman, A.; Saidur, R.J.S.E.M.; Cells, S. MXene based new class of silicone oil nanofluids for the performance improvement of concentrated photovoltaic thermal collector. *Sol. Energy Mater. Sol. Cells* **2020**, *211*, 110526. [[CrossRef](#)]
17. Choi, S.U.; Eastman, J.A. *Enhancing Thermal Conductivity of Fluids with Nanoparticles*; Argonne National Lab.: Lemont, IL, USA, 1995.
18. Saidur, R.; Leong, K.Y.; Mohammed, H.A. A review on applications and challenges of nanofluids. *Renew. Sustain. Energy Rev.* **2011**, *15*, 1646–1668. [[CrossRef](#)]
19. Iranmanesh, S.; Ong, H.C.; Ang, B.C.; Sadeghinezhad, E.; Esmailzadeh, A.; Mehrali, M. Thermal performance enhancement of an evacuated tube solar collector using graphene nanoplatelets nanofluid. *J. Clean. Prod.* **2017**, *162*, 121–129. [[CrossRef](#)]
20. Amani, M.; Amani, P.; Mahian, O.; Estellé, P. Multi-objective optimization of thermophysical properties of eco-friendly organic nanofluids. *J. Clean. Prod.* **2017**, *166*, 350–359. [[CrossRef](#)]
21. Sarkar, J. A critical review on convective heat transfer correlations of nanofluids. *Renew. Sustain. Energy Rev.* **2011**, *15*, 3271–3277. [[CrossRef](#)]
22. Wang, X.Q.; Mujumdar, A.S. Heat transfer characteristics of nanofluids: A review. *Int. J. Therm. Sci.* **2007**, *46*, 1–19. [[CrossRef](#)]
23. Ahmadi, M.H.; Mirlohi, A.; Nazari, M.A.; Ghasempour, R. A review of thermal conductivity of various nanofluids. *J. Mol. Liq.* **2018**, *265*, 181–188. [[CrossRef](#)]
24. Parashar, N.; Aslfattahi, N.; Yahya, S.M.; Saidur, R. *An Artificial Neural Network Approach for the Prediction of Dynamic Viscosity of MXene-Palm Oil Nanofluid Using Experimental Data*; Springer: Berlin, Germany, 2020.
25. Sadri, R.; Ahmadi, G.; Togun, H.; Dahari, M.; Kazi, S.N.; Sadeghinezhad, E.; Zubir, N. An experimental study on thermal conductivity and viscosity of nanofluids containing carbon nanotubes. *Nanoscale Res. Lett.* **2014**, *9*, 151. [[CrossRef](#)]
26. Mesgari, S.; Taylor, R.A.; Hjerrild, N.E.; Crisostomo, F.; Li, Q.; Scott, J. An investigation of thermal stability of carbon nanofluids for solar thermal applications. *Sol. Energy Mater. Sol. Cells* **2016**, *157*, 652–659. [[CrossRef](#)]
27. Yashawantha, K.M.; Asif, A.; Babu, G.R.; Ramis, M.K. Rheological Behavior and Thermal Conductivity of Graphite–Ethylene Glycol Nanofluid. *J. Test. Eval.* **2019**, *49*, 4. [[CrossRef](#)]
28. Chen, W.; Zou, C.; Li, X. Application of large-scale prepared MWCNTs nanofluids in solar energy system as volumetric solar absorber. *Sol. Energy Mater. Sol. Cells* **2019**, *200*, 109931. [[CrossRef](#)]
29. Al-Kahtani, A.A.; Almuqati, T.; Alhokbany, N.; Ahamad, T.; Naushad, M.; Alshehri, S.M. A clean approach for the reduction of hazardous 4-nitrophenol using gold nanoparticles decorated multiwalled carbon nanotubes. *J. Clean. Prod.* **2018**, *191*, 429–435. [[CrossRef](#)]

30. Mehrali, M.; Sadeghinezhad, E.; Akhiani, A.R.; Latibari, S.T.; Talebian, S.; Dolatshahi-Pirouz, A.; Metselaar, H.S.; Mehrali, M. An ecofriendly graphene-based nanofluid for heat transfer applications. *J. Clean. Prod.* **2016**, *137*, 555–566. [[CrossRef](#)]
31. Hajjar, Z.; morad Rashidi, A.; Ghozatloo, A. Enhanced thermal conductivities of graphene oxide nanofluids. *Int. Commun. Heat Mass Transf.* **2014**, *57*, 128–131. [[CrossRef](#)]
32. Mashali, F.; Languri, E.M.; Davidson, J.; Kerns, D.; Johnson, W.; Nawaz, K.; Cunningham, G. Thermo-physical properties of diamond nanofluids: A review. *Int. J. Heat Mass Transf.* **2019**, *129*, 1123–1135. [[CrossRef](#)]
33. Zheng, R.; Gao, J.; Wang, J.; Feng, S.P.; Ohtani, H.; Wang, J.; Chen, G. Thermal Percolation in Stable Graphite Suspensions. *Nano Lett.* **2012**, *12*, 188–192. [[CrossRef](#)]
34. Yu, W.; Xie, H.; Bao, D.J.N. Enhanced thermal conductivities of nanofluids containing graphene oxide nanosheets. *Nanotechnology* **2009**, *21*, 055705. [[CrossRef](#)]
35. Baby, T.T.; Ramaprabhu, S. Investigation of thermal and electrical conductivity of graphene based nanofluids. *J. Appl. Phys.* **2010**, *108*, 124308. [[CrossRef](#)]
36. Wang, F.; Han, L.; Zhang, Z.; Fang, X.; Shi, J.; Ma, W. Surfactant-free ionic liquid-based nanofluids with remarkable thermal conductivity enhancement at very low loading of graphene. *Nanoscale Res. Lett.* **2012**, *7*, 314. [[CrossRef](#)] [[PubMed](#)]
37. Oster, K.; Hardacre, C.; Jacquemin, J.; Ribeiro, A.P.; Elsinawi, A. Thermal Conductivity Enhancement Phenomena in Ionic Liquid-Based Nanofluids (Ionanofluids). *Aust. J. Chem.* **2019**, *72*, 21–33. [[CrossRef](#)]
38. Hosseinghorbani, A.; Mozaffarian, M.; Pazuki, G. Application of graphene oxide IoNanofluid as a superior heat transfer fluid in concentrated solar power plants. *Int. Commun. Heat Mass Transf.* **2020**, *111*, 104450. [[CrossRef](#)]
39. Fredlake, C.P.; Crosthwaite, J.M.; Hert, D.G.; Aki, S.N.; Brennecke, J.F. Thermophysical properties of imidazolium-based ionic liquids. *J. Chem. Eng. Data* **2004**, *49*, 954–964. [[CrossRef](#)]
40. Qeays, I.A.; Yahya, S.M.; Asjad, M.; Khan, Z.A. Multi-performance optimization of nanofluid cooled hybrid photovoltaic thermal system using fuzzy integrated methodology. *J. Clean. Prod.* **2020**, *256*, 120451. [[CrossRef](#)]
41. Abdallah, S.R.; Saidani-Scott, H.; Abdellatif, O.E. Performance analysis for hybrid PV/T system using low concentration MWCNT (water-based) nanofluid. *Sol. Energy* **2019**, *181*, 108–115. [[CrossRef](#)]
42. Aberoumand, S.; Ghamari, S.; Shabani, B. Energy and exergy analysis of a photovoltaic thermal (PV/T) system using nanofluids: An experimental study. *Sol. Energy* **2018**, *165*, 167–177. [[CrossRef](#)]
43. Sardarabadi, M.; Passandideh-Fard, M.; Heris, S.Z. Experimental investigation of the effects of silica/water nanofluid on PV/T (photovoltaic thermal units). *Energy* **2014**, *66*, 264–272. [[CrossRef](#)]
44. Sardarabadi, M.; Passandideh-Fard, M.; Maghrebi, M.-J.; Ghazikhani, M. Experimental study of using both ZnO/water nanofluid and phase change material (PCM) in photovoltaic thermal systems. *Sol. Energy Mater. Sol. Cells* **2017**, *161*, 62–69. [[CrossRef](#)]
45. Ebaid, M.S.Y.; Ghrair, A.M.; Al-Busoul, M. Experimental investigation of cooling photovoltaic (PV) panels using (TiO₂) nanofluid in water -polyethylene glycol mixture and (Al₂O₃) nanofluid in water-cetyltrimethylammonium bromide mixture. *Energy Convers. Manag.* **2018**, *155*, 324–343. [[CrossRef](#)]
46. Hendricks, J.H.; Van Sark, W.G. Annual performance enhancement of building integrated photovoltaic modules by applying phase change materials. *Progress in Photovoltaics: Research and Applications. Prog. Photovolt. Res. Appl.* **2013**, *21*, 620–630.
47. Ghadiri, M.; Sardarabadi, M.; Pasandideh-Fard, M.; Moghadam, A.J. Experimental investigation of a PVT system performance using nano ferrofluids. *Energy Convers. Manag.* **2015**, *103*, 468–476. [[CrossRef](#)]
48. Naguib, M.; Come, J.; Dyatkin, B.; Presser, V.; Taberna, P.L.; Simon, P.; Barsoum, M.W.; Gogotsi, Y. MXene A promising transition metal carbide anode for lithium-ion batteries. *Electrochem. Commun.* **2012**, *16*, 61–64. [[CrossRef](#)]
49. Wang, D.; Lin, Y.; Hu, D.; Jiang, P.; Huang, X. Multifunctional 3D-MXene/PDMS nanocomposites for electrical, thermal and triboelectric applications. *Compos. Part A Appl. Sci. Manuf.* **2020**, *130*, 105754. [[CrossRef](#)]
50. Naguib, M.; Mashtalir, O.; Carle, J.; Presser, V.; Lu, J.; Hultman, L.; Gogotsi, Y. Two-dimensional transition metal carbides. *ACS Nano* **2012**, *6*, 1322–1331. [[CrossRef](#)]
51. Naguib, M.; Halim, J.; Lu, J.; Cook, K.M.; Hultman, L.; Gogotsi, Y.; Barsoum, M.W. New two-dimensional niobium and vanadium carbides as promising materials for Li-ion batteries. *J. Am. Chem. Soc.* **2013**, *135*, 15966–15969. [[CrossRef](#)]

52. Huang, K.; Li, Z.; Lin, J.; Han, G.; Huang, P. Two-dimensional transition metal carbides and nitrides (MXenes) for biomedical applications. *Chem. Soc. Rev.* **2018**, *47*, 5109–5124. [[CrossRef](#)]
53. Lin, H.; Wang, X.; Yu, L.; Chen, Y.; Shi, J. Two-Dimensional Ultrathin MXene Ceramic Nanosheets for Photothermal Conversion. *Nano Lett.* **2017**, *17*, 384–391. [[CrossRef](#)]
54. Lei, J.C.; Zhang, X.; Zhou, Z. Recent advances in MXene: Preparation, properties, and applications. *Front. Phys.* **2015**, *10*, 276–286. [[CrossRef](#)]
55. Ji, J.; Zhao, L.; Shen, Y.; Liu, S.; Zhang, Y. Covalent stabilization and functionalization of MXene via silylation reactions with improved surface properties. *FlatChem* **2019**, *17*, 100128. [[CrossRef](#)]
56. Hunter, R.J. *Zeta Potential in Colloid Science: Principles and Applications*; Academic Press: Cambridge, MA, USA, 2013.
57. Wang, X.; Garnero, C.; Rochard, G.; Magne, D.; Morisset, S.; Hurand, S.; Chartier, P.; Rousseau, J.; Cabioch, T.; Coutanceau, C.; et al. A new etching environment (FeF₃/HCl) for the synthesis of two-dimensional titanium carbide MXenes: A route towards selective reactivity vs. water. *J. Mater. Chem. A* **2017**, *5*, 22012–22023. [[CrossRef](#)]
58. Ghidui, M.; Lukatskaya, M.R.; Zhao, M.-Q.; Gogotsi, Y.; Barsoum, M.W. Conductive two-dimensional titanium carbide ‘clay’ with high volumetric capacitance. *Nature* **2014**, *516*, 78. [[CrossRef](#)] [[PubMed](#)]
59. Xu, G.; Wang, X.; Gong, S.; Wei, S.; Liu, J.; Xu, Y. Solvent-regulated preparation of well-intercalated Ti₃C₂T_x MXene nanosheets and application for highly effective electromagnetic wave absorption. *Nanotechnology* **2018**, *29*, 355201. [[CrossRef](#)]
60. Chen, H.; Chen, N.; Zhang, M.; Li, M.; Gao, Y.; Wang, C.; Chen, G.; Du, F. Ti₃C₂T_x MXene decorated with Sb nanoparticles as anodes material for sodium-ion batteries. *Nanotechnology* **2019**, *30*, 134001. [[CrossRef](#)]
61. Li, Y.; Zhou, X.; Wang, J.; Deng, Q.; Li, M.; Du, S.; Han, Y.H.; Lee, J.; Huang, Q. Facile preparation of in situ coated Ti₃C₂T_x/Ni_{0.5}Zn_{0.5}Fe₂O₄ composites and their electromagnetic performance. *RSC Adv.* **2017**, *7*, 24698–24708. [[CrossRef](#)]
62. Chowdhury, A.; Thynell, S.T. Confined rapid thermolysis/FTIR/ToF studies of imidazolium-based ionic liquids. *Thermochim. Acta* **2006**, *443*, 159–172. [[CrossRef](#)]
63. Arifuzzaman, A.; Ismail, A.F.; Yaacob, I.I.; Alam, M.Z.; Khan, A.A. Stability investigation of water based exfoliated graphene nanofluids. *IOP Conf. Ser. Mater. Sci. Eng.* **2019**, *488*, 012002. [[CrossRef](#)]
64. Otanicar, T.P.; Phelan, P.E.; Prasher, R.S.; Rosengarten, G.; Taylor, R.A. Nanofluid-based direct absorption solar collector. *J. Renew. Sustain. Energy* **2010**, *2*, 033102. [[CrossRef](#)]
65. Clogston, J.D.; Patri, A.K. Zeta potential measurement. In *Characterization of Nanoparticles Intended for Drug Delivery*; Springer: Berlin, Germany, 2011; pp. 63–70.
66. Han, R.; Ma, X.; Xie, Y.; Teng, D.; Zhang, S. Preparation of a new 2D MXene/PES composite membrane with excellent hydrophilicity and high flux. *RSC Adv.* **2017**, *7*, 56204–56210. [[CrossRef](#)]
67. Padmanabhan, S.; Kim, M.; Blanch, H.W.; Prausnitz, J.M. Solubility and rate of dissolution for Miscanthus in hydrophilic ionic liquids. *Fluid Phase Equilibria* **2011**, *309*, 89–96. [[CrossRef](#)]
68. Mashali, F.; Languri, E.; Mirshekari, G.; Davidson, J.; Kerns, D. Nanodiamond nanofluid microstructural and thermo-electrical characterization. *Int. Commun. Heat Mass Transf.* **2019**, *101*, 82–88. [[CrossRef](#)]
69. Singh, V.; Gupta, M. Characterisation and Zeta Potential Measurements of CuO–Water Nanofluids. In *Advances in Interdisciplinary Engineering; Lecture Notes in Mechanical Engineering*; Springer: Singapore, 2019; pp. 741–747.
70. Said, Z.; Abdelkareem, M.A.; Rezk, H.; Nassef, A.M.; Atwany, H.Z. Stability, thermophysical and electrical properties of synthesized carbon nanofiber and reduced-graphene oxide-based nanofluids and their hybrid along with fuzzy modeling approach. *Powder Technol.* **2020**, *364*, 795–809. [[CrossRef](#)]
71. Chen, W.; Qiu, L.; Liang, S.; Zheng, X.; Tang, D. Measurement of thermal conductivities of [mmim]DMP/CH₃OH and [mmim]DMP/H₂O by freestanding sensor-based 3 ω technique. *Thermochimica Acta* **2013**, *560*, 1–6. [[CrossRef](#)]
72. Akhavan-Zanjani, H.; Saffar-Avval, M.; Mansourkiaei, M.; Ahadi, M.; Sharif, F. Turbulent Convective Heat Transfer and Pressure Drop of Graphene–Water Nanofluid Flowing Inside a Horizontal Circular Tube. *J. Dispers. Sci. Technol.* **2014**, *35*, 1230–1240. [[CrossRef](#)]
73. Liu, J.; Wang, F.; Zhang, L.; Fang, X.; Zhang, Z. Thermodynamic properties and thermal stability of ionic liquid-based nanofluids containing graphene as advanced heat transfer fluids for medium-to-high-temperature applications. *Renew. Energy* **2014**, *63*, 519–523. [[CrossRef](#)]

74. Lee, G.-J.; Rhee, C.K. Enhanced thermal conductivity of nanofluids containing graphene nanoplatelets prepared by ultrasound irradiation. *J. Mater. Sci.* **2014**, *4*, 1506–1511. [[CrossRef](#)]
75. Sang, L.; Ai, W.; Wu, Y.; Ma, C. Enhanced specific heat and thermal conductivity of ternary carbonate nanofluids with carbon nanotubes for solar power applications. *Int. J. Energy Res.* **2020**, *44*, 334–343. [[CrossRef](#)]
76. Tiznobaik, H.; Shin, D. Enhanced specific heat capacity of high-temperature molten salt-based nanofluids. *Int. J. Heat Mass Transf.* **2013**, *57*, 542–548. [[CrossRef](#)]
77. Ghazvini, M.; Akhavan-Behabadi, M.A.; Rasouli, E.; Raisee, M. Heat transfer properties of nanodiamond–engine oil nanofluid in laminar flow. *Heat Transf. Eng.* **2012**, *33*, 525–532. [[CrossRef](#)]
78. Oster, K.; Hardacre, C.; Jacquemin, J.; Ribeiro, A.P.C.; Elsinawi, A. Understanding the heat capacity enhancement in ionic liquid-based nanofluids (ionanofluids). *J. Mol. Liq.* **2018**, *253*, 326–339. [[CrossRef](#)]
79. Elhamarnah, Y.A.; Nasser, M.; Qiblawey, H.; Benamor, A.; Atilhan, M.; Aparicio, S. A comprehensive review on the rheological behavior of imidazolium based ionic liquids and natural deep eutectic solvents. *J. Mol. Liq.* **2019**, *277*, 932–958. [[CrossRef](#)]
80. Aravind, S.S.J.; Baskar, P.; Baby, T.T.; Sabareesh, R.K.; Das, S.; Ramaprabhu, S. Investigation of Structural Stability, Dispersion, Viscosity, and Conductive Heat Transfer Properties of Functionalized Carbon Nanotube Based Nanofluids. *J. Phys. Chem. C* **2011**, *115*, 16737–16744. [[CrossRef](#)]
81. Ko, G.H.; Heo, K.; Lee, K.; Kim, D.S.; Kim, C.; Sohn, Y.; Choi, M. An experimental study on the pressure drop of nanofluids containing carbon nanotubes in a horizontal tube. *Int. J. Heat Mass Transf.* **2007**, *50*, 4753. [[CrossRef](#)]
82. Adam, S.A.; Ju, X.; Zhang, Z.; Lin, J.; El-Samie, M.M.A.; Xu, C. Effect of temperature on the stability and optical properties of SiO₂-water nanofluids for hybrid photovoltaic/thermal applications. *Appl. Therm. Eng.* **2020**, *175*, 115394. [[CrossRef](#)]
83. Sardarabadi, M.; Passandideh-Fard, M. Experimental and numerical study of metal-oxides/water nanofluids as coolant in photovoltaic thermal systems (PVT). *Sol. Energy Mater. Sol. Cells* **2016**, *157*, 533–542. [[CrossRef](#)]
84. Lee, J.H.; Hwang, S.G.; Lee, G.H. Efficiency Improvement of a Photovoltaic Thermal (PVT) System Using Nanofluids. *Energies* **2019**, *12*, 3063. [[CrossRef](#)]



© 2020 by the authors. Licensee MDPI, Basel, Switzerland. This article is an open access article distributed under the terms and conditions of the Creative Commons Attribution (CC BY) license (<http://creativecommons.org/licenses/by/4.0/>).